nature catalysis

REVIEW ARTICLE

https://doi.org/10.1038/s41929-019-0364-x

Control of metal-support interactions in heterogeneous catalysts to enhance activity and selectivity

Tom W. van Deelen[1,2], Carlos Hernández Mejía[1,2] and Krijn P. de Jong[1]*

Metal nanoparticles stabilized on a support material catalyse many major industrial reactions. Metal-support interactions in these nanomaterials can have a substantial influence on the catalysis, making metal-support interaction modulation one of the few tools able to enhance catalytic performance. This topic has received much attention in recent years, however, a systematic rationalization of the field is lacking due to the great diversity in catalysts, reactions and modification strategies. In this review, we cover and categorize the recent progress in metal-support interaction tuning strategies to enhance catalytic performance for various reactions. Furthermore, we quantify the productivity enhancements resulting from metal-support interaction control that have been achieved in C_1 chemistry in recent years. Our analysis shows that up to fifteen-fold productivity enhancement has been achieved, and that metal-support interaction is most impactful for metal nanoparticles smaller than four nanometres. These findings demonstrate the importance of metal-support interaction to improve performance in catalysis.

Metal nanoparticles are the key functional component in various nanotechnological applications, owing to the unique properties that arise from their size, shape and composition[1,2]. Consequently, several strategies have been developed to design and control these properties. A key strategy is to immobilise nanoparticles on a support to enhance their stability and control their spatial distribution[3,4]. However, supports are typically not inert and the interaction with nanoparticles gives rise to new interface phenomena. Such metal-support interaction (MSI) may have a profound impact on the resulting performance of the metal nanoparticles[5,6]. Hence, strategies for controlling these interactions to optimize performance are highly desirable.

In heterogeneous catalysis, MSI affects the catalytic performance and its regulation thus provides options for catalyst design. Recently, the topic has gained much attention, as judged by the increasing number of reports on the subject, and substantial progress has been made in the methodology to tune metal-support interactions, with the aim to improve the performance of supported metal catalysts. Because of the great diversity in MSI tuning approaches, catalytic systems and reactions, a systematic and critical overview would be helpful to determine the most effective tuning strategies for real working catalysts.

This review starts with a brief introduction covering the relevant concepts of MSI phenomena and the following sections discuss the latest reports on MSI tuning strategies for catalysis, systematically arranged after the different stages of catalyst modification. Several interesting reviews have already been published in the field of MSI[7–10]. In comparison, we have reviewed the literature published since 2015 on tuning interactions between metals and supports to improve catalytic performance, covering mainly three-dimensional catalysts containing metal nanoparticles or clusters under industrially relevant conditions. For a general discussion, we provide a quantitative analysis of the scale of performance enhancement that has been reported in past years. To quantify the effects of MSI modulation on catalytic performance, we focus on intrinsic activity and selectivity as performance descriptors, and less on stability. Although highly relevant from an application point of view, activity enhancement due to changes in metal dispersion (increased metal specific surface area) are not covered here. Relative scaling factors are obtained by comparing the productivities of tuned and reference catalysts in C_1 chemistry, which allow us to point out the most successful tuning strategies and opportunities in this field.

Metal-support interactions

Impact on catalysis originates from interactions between metal nanoparticles and their supporting matrix (Fig. 1a). Typical metal-support phenomena relate to charge transfer, the interfacial perimeter, nanoparticle morphology, chemical composition and strong metal-support interaction (SMSI). These phenomena are often entangled and some will have a stronger influence than others, depending on the catalyst and the reaction.

Charge transfer. The interface between a metal nanoparticle (NP) and the support can give rise to a rearrangement of electrons within both materials[5]. Redistribution of electrons with noticeable effects is limited to a couple of atomic layers at the interface and might be accompanied, in some cases, by a change in oxidation state of the metal atoms from the nanoparticle or of the support's metal ions[11,12]. The magnitude and direction of the charge transfer is driven by differences in the Fermi level of the metal NP and the support, ultimately seeking equilibration of the electron chemical potentials. The metallic character of the NPs enables electron mobility, however their size is relevant in the nanometre regime, since the smaller the NP the more localized are its electronic states. Several characteristics of the support are important for charge transfer, such as its conductivity, reducibility, exposed crystal planes, morphology and occurrence of defects[13,14].

Interfacial perimeter. Interface sites at the perimeter of the NP are a unique environment, given that they are in direct contact with the

[1]Inorganic Chemistry and Catalysis, Debye Institute for Nanomaterials Science, Utrecht University, Utrecht, The Netherlands. [2]These authors contributed equally: Tom W. van Deelen, Carlos H. Mejía. *e-mail: k.p.dejong@uu.nl

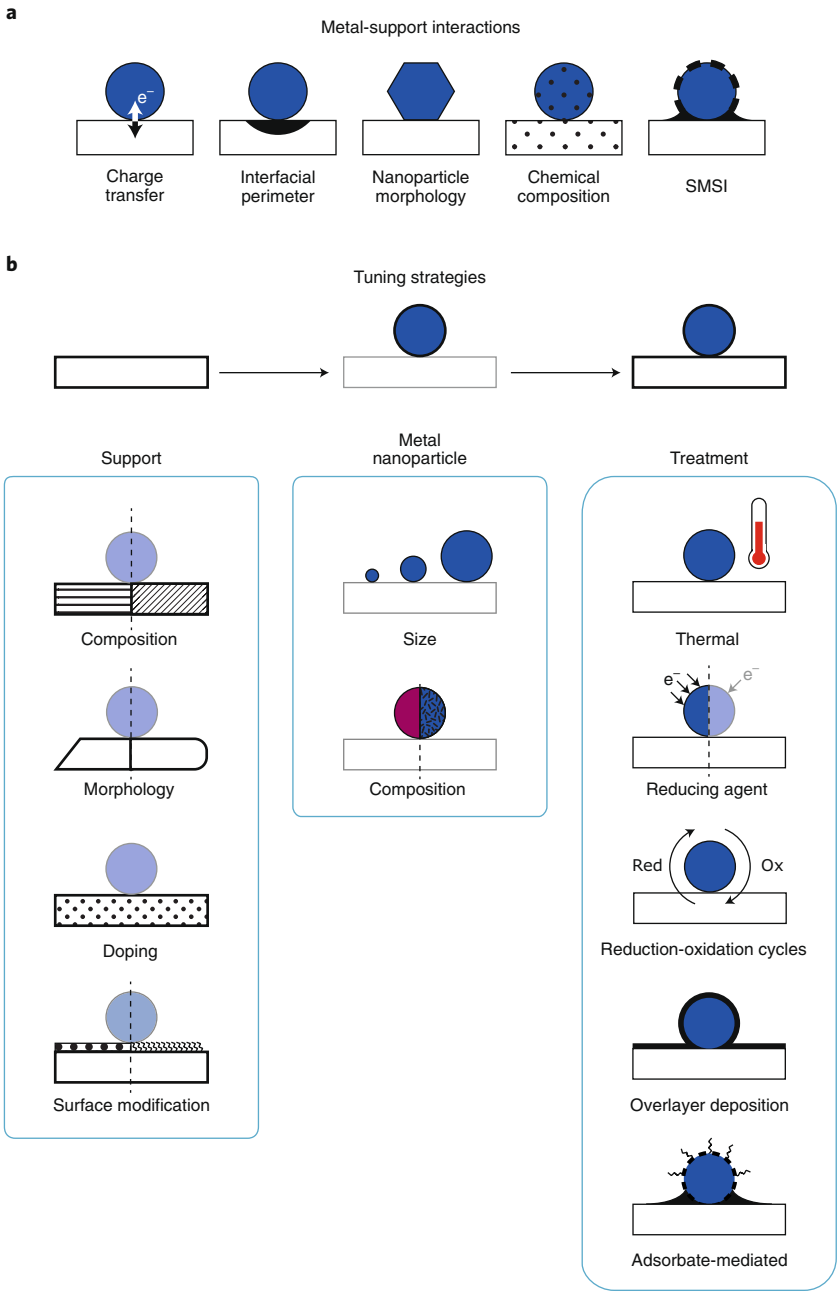

Fig. 1 | Schematic representation of main metal-support interactions and their tuning strategies. a, The five main phenomena of metal-support interactions are shown. **b**, The approaches for tuning such interactions are shown and divided after the different stages of catalyst modification, that is, via solely the support or the nanoparticle or via treatments on the metal-support composite material.

NP, the support and the reactants, facilitating synchronized reactions[15,16]. Furthermore, it has been shown that upon charge transfer, atoms at the perimeter favour the accumulation of excess charges[17]. All this can significantly enhance adsorption and reactions of molecules at the perimeter[18,19]. Additionally, the close proximity of the nanoparticle to different functionalities or defects at the surface of the support (for example, oxygen vacancies, hydroxyl groups, Lewis acids or bases) might also aid local sequential reactions or stabilize transition states of reactants or products[20,21].

Spillover via the interfacial perimeter can occur as well. This initiates with the activation of a reactant on one surface, typically on the metal NP, which is then transferred to the other surface, for example, the support. Note that this second surface does not activate the reactants itself under the same conditions. The most studied spillover is for hydrogen, and, to a lesser extent, oxygen or other molecules (for example, CO, $-OCH_3$, and so on). Spillover from the support to the metal nanoparticle can also occur, referred to sometimes as reverse spillover[22–24]. The nature of the support is crucial for spillover; whereas hydrogen spillover on reducible supports occurs fast and at relatively large distances, it has been shown to proceed ten orders of magnitude slower on non-reducible supports and it is restricted to short distances[25].

NP morphology. The shape and crystal structure of nanoparticles has a strong influence on their catalytic performance, considering that different shapes expose certain facets, and that these facets can

have favourable or unfavourable configurations of atoms[26,27]. The adhesion energy at the metal-support interface affects the shape of the nanoparticles[26,28]. In general, supports with stronger adhesion result in particles with more faceted and sometimes raft-like shapes[29]. A trend observed for metal oxide supports suggests that adhesion energies increase with increasing heat of formation of the most stable oxide of the metal[30] and by decreasing the metal NP's size[31]. Besides NP shape, high adhesion energy will also reduce the mobility of the NPs and hence their tendency to grow[6,32].

The equilibrium shape of a metal NP is often determined by minimization of its total surface free energy. Contact with the support can lower the surface energy of certain NP planes, favouring some shapes over others. The surface energy of a metal can also change under reaction conditions upon adsorption of a gas, where the change in its surface energy tends to affect the contact surface area with the NP, and hence modifies the NP's shape[33,34]. Moreover, a misfit between the lattices of the support and the nanoparticle can generate strain and defects, modifying the morphology of the NP[35]. Additionally, the effect of lattice mismatching is more pronounced for smaller metal nanoparticles, as observed for gold nanoparticles smaller than three nanometres supported on titania[36].

Chemical composition. A solid-state reaction can take place between metal NPs and the support resulting in the formation of new phases. Exchange of species is possible in both directions, usually coupled with a redox process, with oxidation of the metal atoms from the nanoparticle or reduction of metal ions from the support. This phenomenon has ambivalent consequences, since the resulting species can both lower or enhance catalytic performance. On the one hand, formation of inactive phases, such as mixed metal oxides (for example, metal aluminates), at the expense of active metal sites has been recognized for long time as a prominent deactivation process[37,38]. On the other hand, formation of highly active intermetallic nanoparticles is also possible by reduction of metal or metalloid ions from the support to incorporate into the metal NP. This phenomenon has recently attracted significant attention and is sometimes referred as reactive metal-support interaction (RMSI)[39]. The pre-deposited metal nanoparticles aid in the activation of the support. On high temperatures and reductive conditions, the former cations from the support can migrate to the nanoparticle. This can be facilitated by doping the support or employing two-dimesional supports. The strategy has been effectively applied to incorporate difficult-to-reduce metals or metalloids (for example, Si, Al, V, Ti, Nb and so on) into late transition metal NPs, resulting in novel catalytic systems[40].

The local composition of alloyed metal nanoparticles can be affected by interacting with the support, where re-arrangement of the components in an alloyed nanoparticle is driven by preferential interaction of one of its elements with the support at the interface[41]. This can lead to compositional rearrangements different from the initially uniform composition, such as core-shell or segregated subcluster structures, affecting the synergy of the metals and hence their catalytic performance[42,43].

Strong metal-support interaction. The term strong metal-support interaction refers to metal NP coverage by suboxides, which are generated from the support under reducing conditions[44,45]. The phenomenon is driven by minimization of the high surface energy of the metal NP by mobile support suboxide species. High surface energy metals that are capable of activating hydrogen are prone to encapsulation, and reducible supports are necessary to generate the suboxide species. The suboxides covering the nanoparticle consist of a few atomic layers with probably amorphous character and possess dynamic structures under different gas atmospheres, as shown in the case of titanium and iron oxide[46–48]. Extensive coverage of the NP is detrimental for the catalytic performance due to blockage of active sites. However, these suboxides can change the (local) electronic structure of the metal surface and act as Lewis acids, thereby promoting the activation of reactants and improve the catalytic performance[49].

Modification of metal-support interactions. The aforementioned MSI phenomena can have a major impact on the catalytic performance. Therefore, modification of MSI can be employed as a tool for the design of catalytic systems with enhanced performance. Several synthetic strategies for the control of the MSI have been reported, which can be classified according to changes to the catalyst's components before and after assembly of the composite material (Fig. 1b). Through this distinction, we aim to emphasize the similarities within one strategy, when applied to different families of catalysts, supports and reactions. In the coming section, we start by discussing reports targeting modification mainly of the support, divided into strategies involving support composition, morphology, doping and surface modifications. Thereafter, strategies that focus on nanoparticle modifications are discussed, particularly changes in NP's size and composition. Lastly, we cover the approaches to tune MSI on the as-prepared catalyst by use of a treatment. The identified treatments include thermal, reducing agent, reduction-oxidation cycles, overlayer deposition and adsorbate-mediated treatments.

Support

The first approach to tune the metal-support interactions is through a judicious choice of support characteristics. The support provides numerous opportunities for changing its structure and surface composition, making it one of the most employed handles to tune MSI. In this section, we will discuss modifications of supports before the deposition of NPs. Support tuning strategies after NP loading are classified as a post-synthesis treatment and will be discussed in the treatment section.

Support composition. The first point of consideration is the chemical composition of the support, as that partially defines the starting point for MSI. The discussion of support composition involves comparisons between different types of supports, as well as between different chemical compositions of related support compounds. Examples of support properties impacting MSI include the surface composition of the support (such as extent of hydroxylation), the electronic structure of the support (especially important for electro- or photocatalysis), ion mobility (for example, formation of oxygen vacancies or cation diffusion), reactivity of the support, and the possibility to segregate cations to form intermetallic compounds.

Several recent publications investigated the role of the support in the catalytic oxidation of CO by Au NPs. Saavedra and co-workers[50] studied, in detail, the origin of the lower CO oxidation activity seen at room temperature with Au NP supported on Al_2O_3 compared to TiO_2. They concluded that the activity was, to a large extent, determined by competitive adsorption of water (promoting) and carbonates (poisoning) on the support and active metal sites. The role of the support was mainly to supply adsorbed water to the Au NPs. This was more efficient on TiO_2, given that carbonates bind more strongly to Al_2O_3 than to TiO_2, and the authors proposed that oxygen vacancies do not participate significantly in the catalysis. Contrary, Wang and colleagues[51,52] reported that oxygen vacancies are generated in TiO_2, and that these vacancies are mainly responsible for the modified catalytic activity. The vacancies caused overall electron donation to the Au NPs, making these NPs negatively charged. The charge donation resulted in strongly modified CO adsorption strength and lower intrinsic activity at 80 °C. Interestingly, the TOF could be enhanced by one order of magnitude by re-oxidation of the catalyst, which reduced the amount of oxygen vacancies. One possibility for these two different explanations of the same catalytic system could be the different pre-treatment or reaction conditions,

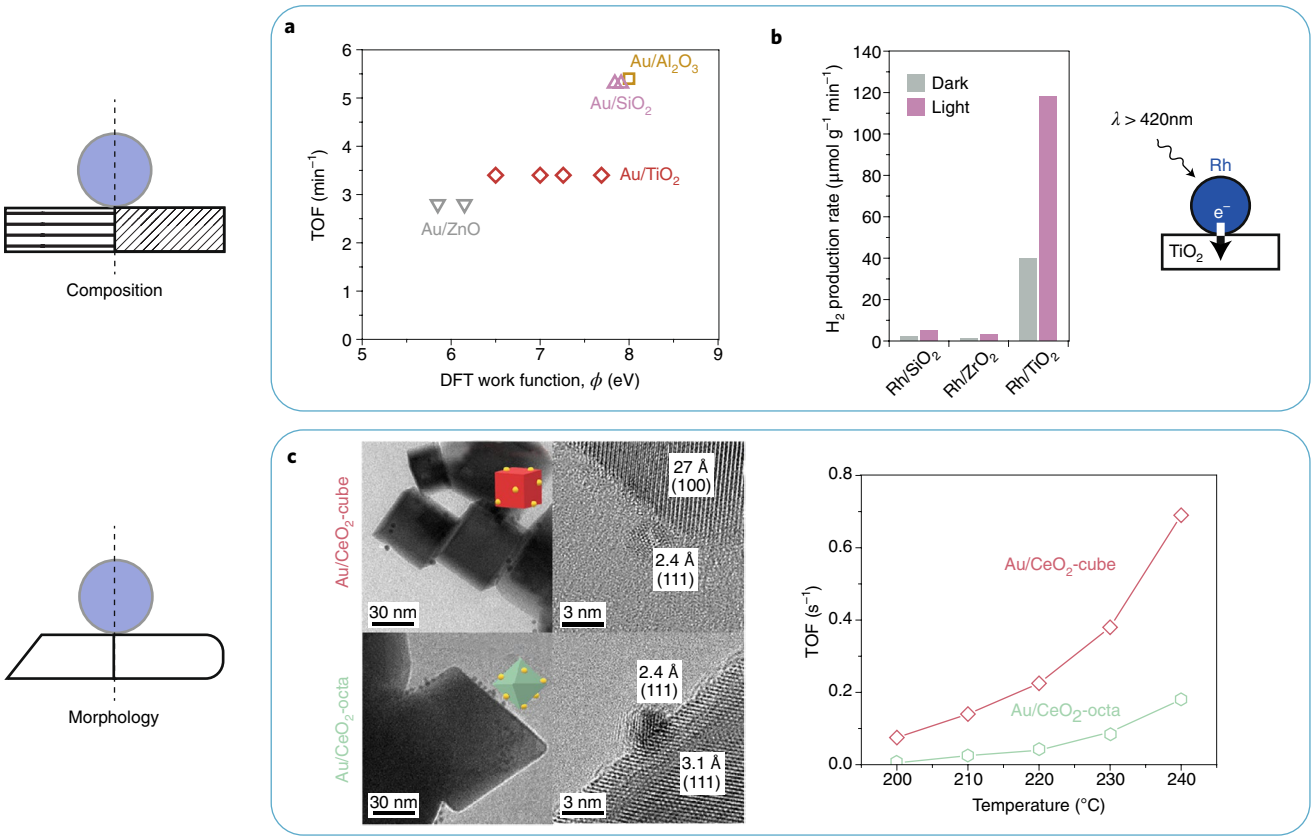

Fig. 2 | MSI tuning strategies involving modification of the support composition and morphology. a, TOF for benzyl alcohol selective oxidation plotted against the work function of the supports, which is the inverse of the support's electron-donating ability to gold NPs. Multiple work function values were obtained for some supports, because these values were calculated for individual support crystal facets. Adapted from ref. [53], Springer Nature Ltd. **b**, Methane steam reforming activity expressed as H_2 production rate for Rh NPs supported on SiO_2, ZrO_2 and TiO_2 with and without exposure to visible light adapted from ref. [54], American Chemical Society. **c**, Use of different ceria morphologies (cubes or octahedra) as support for gold NPs and their effect on CO oxidation. Adapted from ref. [70], American Chemical Society.

such as reaction temperature (RT versus 80 °C), feed composition (1 versus 20 % O_2), or dilution with inert SiC. For example, it has been reported that the mechanism of CO oxidation changes with reaction temperature[52].

The activity for benzyl alcohol oxidation followed the opposite trend as for CO oxidation, with the intrinsic activity decreasing in the order Au/Al_2O_3>Au/SiO_2>Au/TiO_2>Au/ZnO[53] (Fig. 2a). Charge transfer occurred to a different extent from various supports to Au NPs of 2–4 nm size and correlated inversely with the electron donation capacity of the support. Hydride transfer from the alcohol to Au was argued to be the rate determining step in this case, and would account for lower activity of more negatively charged Au NP.

In photocatalysis, a semiconductor support's bandgap of appropriate size and position facilitates light absorption and transfer of the generated charge to, or from, metal NPs performing catalysis. The activity of Rh/TiO_2 in the steam reforming of methane was already 13 times higher than that of Rh/SiO_2 and Rh/ZrO_2 in dark conditions, and the activity of Rh/TiO_2 was enhanced to nearly three times greater when it was exposed to light (Fig. 2b)[54]. However, the opposite has been observed as well; Pt/Ta_2O_5 was more active than Pt/TiO_2 for 2-propanol oxidation to acetone, because hot electrons generated on the Pt NPs were not transferred to the support, and hence drove the catalysis on the Pt NPs[55]. X-ray photoelectron spectroscopy (XPS) analysis indicated that the Pt phase was more negatively charged on Ta_2O_5 than on other supports. Similar considerations also apply to electrocatalysis. The activity of Pt NPs for electrocatalytic reduction of oxygen was significantly enhanced when a mixture of boron carbide and graphite was used as support instead of pure graphite and it was argued that this was solely an electronic effect[56].

Perovskites are a class of metal oxides with the general formula ABO_3, in which a large variety of metal ions can be incorporated in the A- and B-sites of their crystal structures. Some of these ions can be extracted from the perovskite lattice upon reduction to form nanoparticles. This approach has received great attention for electrochemical systems[57], mainly due to the beneficial conductive properties of perovskites for electrodes. However, this approach has been employed to a lesser extent for catalysis, due to the resulting low metal loading and limitation to easy-to-reduce metal ions, such as noble metals. Recently, non-stoichiometric perovskites with A-site deficiency extended the range of metal ions capable of forming nanoparticles to more difficult to reduce metal ions (for example, Ti^{4+}, $Fe^{2+/3+}$, $Mn^{2+/3+}$, Ni^{2+})[58,59]. The resulting nanoparticles resisted the harsh conditions of methane reforming due to partial embedding in the support, avoiding the formation of carbon fibres at the periphery of the nanoparticles. Formation of alloyed nanoparticles is also possible by use of this strategy. Alloyed Pt_3Ni nanoparticles obtained from $La_{0.9}Mn_{0.9}Pt_{0.075}Ni_{0.025}O_x$ perovskite have shown high activity for the electrocatalytic oxygen reduction reaction[60]. The strong connection with the conductive perovskite, uniform NP distribution and small NP size for the obtained particles were beneficial to the measured activity.

The disadvantage, however, of using perovskites to form nanoparticles in catalysis is the low specific surface area of these

compounds, due to the high temperatures needed to synthesize the perovskites. Progress has been achieved in fabricating high surface area perovskites by templating methods, however, the challenge remains in the form of the high temperatures needed to form the metal nanoparticles, which usually leads to collapse of the pore structure of the perovskites[61].

Support morphology. Various allotropes or morphologies can exist for one type of support. We will discuss these two properties together, because they are often interrelated and exert a combined effect. For example, the crystal structure and morphology of the support jointly determine the facets that are exposed at the surface of the support, and thereby regulate the local environment for the metal nanoparticles. In this section, we will highlight some recent examples of how the crystal structure of metal oxides can direct NP shape and SMSI, and how shaped support particles can expose special surface sites or confine NPs.

The crystal structure of metal oxides can affect the NPs deposited onto it by directing the shape of the metal NPs. For example, when Pd/Al_2O_3 (α, γ and θ) catalysts were investigated for methane oxidation, the crystal structure of the support affected the shape of Pd NPs, with more distorted NPs on γ-Al_2O_3 and more regularly shaped and facetted NPs on α- and θ-Al_2O_3 (ref. [62]). The shape of the NP together with NP size determined the number of step sites, which could be correlated with intrinsic activity. The presence of pentacoordinate Al^{3+}-sites on the surface of γ-Al_2O_3, as observed by nuclear magnetic resonance, and their absence in α- and θ-Al_2O_3 were proposed to distort the NP shape and increase the TOF of 7.5 nm NP from 0.1 to 0.6 s^{-1}. A similar effect was observed for Pt NPs on γ-Al_2O_3 and CeO_2 (ref. [35]). Especially on CeO_2, the authors were able to show that epitaxial NP growth, dictated by the support crystal structure, directed the shape of the NPs and caused strain. From theoretical investigations, the predicted intrinsic activity for CO oxidation varied between $2x10^{-3}$ and $5x10^{-3}$ s^{-1}, with the occurrence of specific Pt surface sites related to the shape and strain of these NPs.

In addition, one crystal structure can be more susceptible to partial reduction and SMSI. In the case of TiO_2-supported Ru-promoted cobalt catalysts for the Fischer–Tropsch synthesis[63] and rhodium catalysts for steam reforming of propane[64], suboxide coverage was more extensive on TiO_2 in the anatase phase than in the rutile phase. In both cases, the overall activity of the catalysts was higher on rutile, because of fewer blockages of active sites by the TiO_x species. Furthermore, the specific surface area of the TiO_2-anatase support was shown to also influence the extent of SMSI and activity on Ru-Co/TiO_2 catalysts for the Fischer–Tropsch synthesis[65] and Ru/TiO_2 catalysts for CO methanation[66]. The cobalt-weight-based activity decreased for both catalysts with increasing specific surface area of the support, again because of a larger number of blocked sites. The TOF was, however, not affected by the support-specific surface area. In this case, the anatase supports with higher surface area displayed a higher concentration of defects, as inferred from Raman spectroscopy, and this probably led to more facile formation of TiO_x species during reduction.

The shape of the support, that is, the exposed crystal facets, also influence the catalytic performance through MSI. The activity of Pt/TiO_2 for methanol oxidation[67], Co/CeO_2 and Ru/CeO_2 for ammonia synthesis[68,69], and Au/CeO_2 (Fig. 2c) and Au/ZnO for CO oxidation[70,71] showed large differences depending on the facets on which the metal NPs were situated. The facets were controlled by synthesizing nanostructured support particles of controlled shapes. The reason for the modified catalytic performance varied, however, from facilitated reactant/intermediate binding and charge transfer (Pt/TiO_2), enhanced support reduction (Co and Ru on CeO_2) to the occurrence of more vacancies (Au on CeO_2 and ZnO). For Au/ZnO, the vacancies allowed Au to replace Zn in the ZnO crystal lattice and promote a Mars–Van Krevelen mechanism through the formation of Au–O–Au_{Zn} bonds, which are broken more easily than Au–O–Zn bonds. This led to a remarkable 150 times increase in specific activity, which was amplified using a very low activity reference catalyst (see Supplementary Table 1, entry 6).

One- and two-dimensional supports can give rise to confinement, or exposure, of special sites on the support surface. For example, Zhu and co-workers[72] demonstrated enhanced CO oxidation activity for Pt NPs supported on boron nitride nanosheets. The NPs associated with B-vacancies displayed lower electron density, while N-vacancies donated electron density to Pt NPs. As the N-vacancies were the main Pt-binding sites, the Pt NPs were electron rich compared to those supported on bulk boron nitride, which contained fewer vacancies. This enhanced O_2 adsorption and increased CO oxidation activity from 30 to 70 % conversion at 47 °C. Similarly, the selectivity towards CH_4 of Ni NPs on planar siloxenes in CO_2 hydrogenation was 90 % when the NPs were confined in the interior of the siloxenes structures, and 53 % when the Ni NPs were located on the exterior of the support[73]. In this case, confinement tuned the balance between the formate and the CO intermediate reaction pathway. Another example is confinement of Pt NPs in the interior of carbon nanotubes (CNT), which reduced NP size and prevented oxidation of Pt (ref. [74]). This kept the metal in the active state and increased toluene oxidation activity from 4 to 27 μmol g_{Pt}^{-1} s^{-1} at 140 °C, compared to NPs located on the exterior surface of the CNT.

Two-dimensional early transition metal carbides present weaker metal–carbon bonds, due to their dimensionality, compared to bonds in traditional metal oxides or metal carbides. This results in increased chemical reactivity of the metal ions and facilitates RMSI. A two-dimensional niobium carbide Nb_2CT_x (where T accounts for various elements/groups) has been used as support for platinum nanoparticles and applied for the water–gas shift reaction[75]. The two-dimensionality of this carbide material aided in the formation of a Pt–Nb surface alloy by H_2 reduction at 350 °C. Furthermore, the removal of functional groups (T) such as –OH, –O and –F, exposed terminal niobium sites that were identified as interfaces for H_2O activation. These exposed niobium atoms in contact with the Pt–Nb surface alloy showed strong affinities for H_2O or OH, as indicated by the WGS kinetics. However, this catalyst showed a similar reaction rate of ~$1.5x10^{-2}$ mol_{H2} mol_{Pt}^{-1} s^{-1} as a Pt/Al_2O_3 reference catalyst. Zhu's research group has employed this material, platinum supported on niobium carbide (Pt/Nb_2CT_x), as well as platinum supported on titanium carbide (Pt/$Ti_3C_2T_x$), as catalysts for dehydrogenation of light alkanes[76]. In this case, Pt–Ti (Pt_3Ti) or Pt–Nb (Pt_3Nb) alloy formation increased selectivity towards propene from 60 to ~95 % at 15 % conversion, through facilitating olefin desorption, which prevented secondary reactions.

The amount of literature on tuning MSI via support morphology for electro- or photo-catalysis is limited. This can be rationalized by considering that this strategy often concerns metal oxides with limited conductivity. One exception is the work by Shi and co-workers[77] on Au NPs supported on disordered TiO_2 rich in oxygen vacancies, that is, black titania. They found that the presence of intermediate energy levels within the band gap enhanced trapping of hot plasmonic electrons from gold and increased the photocurrent densities from 126 to 280 μA cm^{-1}, with respect to Au on regular white TiO_2, making photocatalytic water splitting more efficient.

Doping. Doping of supports with elements of different valency mainly serves to regulate the electronic structure of the support (and metal NP), and typically results in enhanced or reduced electron donating properties.

Doping of carbons is an active field, especially for electrochemical applications such as batteries and supercapacitors and metal-free catalysis. When used as a support material for metallic nanoparticles, carbon can be doped with a variety of heteroatoms, of which

N is most investigated. For a more comprehensive overview of how this strategy can be applied to obtain the desired reactivities, we refer to a recent review[78]. Here, we will cover the basics and highlight two studies which we believe illustrate the concept and possibilities.

N-doping is often reported to increase the support-metal nanoparticle binding strength, and therefore leads to smaller NPs and higher stabilities[79]. Incorporating N in a carbon matrix can have various effects on its electronic structure, depending on the position of incorporation (for example, pyrrolic, pyridinic or graphitic). Ning and co-workers[80] investigated the electronic effect of different N species interacting with Pt nanoparticles of 2–4 nm, and found that pyridinic N acted as an electron acceptor and graphitic N functioned as an electron donor for the Pt nanoparticles. The electron-enriched Pt NPs (in contact with graphitic N) gave the highest activity in electro-oxidation reactions of glycerol and formic acid. The high activity was partially related to an increased rate of CO removal, which otherwise poisons the catalyst. On the other hand, the electron-deficient Pt NPs (in contact with pyridinic N) showed the highest activity in ammonia borane hydrolysis. For both the electron-rich and -deficient NPs, the modified electronic structure was proposed to tune the Pt-reactant bonds, thereby optimizing reactant activation.

The application of carbon nitride with a stoichiometry of C_2N can be considered one of the most extreme cases of N-doping of a support[81]. These materials have a higher standard electrochemical potential than gold and are therefore termed noble carbons[82]. This means that even gold is electron deficient, when supported on C_2N, resulting in active materials for ammonia synthesis via electrocatalytic reduction of nitrogen[83]. The positive effect of the C_2N support on catalysis was more pronounced when gold was dispersed as single atoms compared to nanoparticles, because of maximal MSI in the case of atomically dispersed metal.

Doping of a magnesium aluminate spinel support with Fe was investigated to improve the performance of a supported Ni catalyst for dry reforming of methane[84]. During the reduction process, Ni catalysed the reduction of Fe from the support, most probably via H-spillover and, as a result, up to 50 % Fe was extracted from the support and an Ni–Fe alloy was formed at the NP surface. At an Fe/Ni ratio of ~10, carbon (coke) formation was inhibited. Interestingly, doping (Fe incorporated in the spinel) was more effective than surface modification (Fe on the surface of spinel), demonstrating the importance of the residual Fe ions left in the spinel structure of the $MgFe_xAl_{2-x}O$ support.

Doping γ-Al_2O_3 with Mg^{2+} ions before the introduction of Ni partially prevented undesired mixed metal oxide formation during dry reforming of methane[85]. This left more metallic Ni surface area available for catalysis and reduced deactivation. In addition, coke formation was suppressed, although that was mainly ascribed to the presence of small (~2 nm) Ni particles. Recently, a related study on Ni-based catalysts for dry methane reforming was conducted, focusing on doping the Al_2O_3 with La^{3+} ions[86]. The addition of La^{3+} had several effects on catalysis, such as increased activity at La^{3+} loadings between two and ten weight per cent, and decreased selectivity towards coke formation, resulting in increasing stability with La^{3+} content. The positive influence of La^{3+} was ascribed to the introduction of basic sites and stronger MSI. It is quite possible that doping with Mg^{2+} and La^{3+} affects catalytic performance via the same mechanisms, as both form basic oxides, which may counteract the typically acidic nature of γ-Al_2O_3.

Adding cationic or anionic dopants to reducible supports such as TiO_2 can increase their conductivity, making them more attractive supports for electrocatalysis. When both types of dopants were applied simultaneously, more charge transfer to three nanometre Pt NPs was observed[87]. This resulted in three to five times higher Pt mass specific activity in electrocatalytic oxygen reduction than obtained with only one dopant (Fig. 3a). Similarly, an increase in charge transfer from Fe^{3+}-doped ZnO to Pt NPs reportedly led to a five-fold increase in TOF in CO oxidation[88]. Other examples of dopants that affect oxygen vacancies or charge transfer in reducible supports are available[89–91]. Furthermore, Schumann and co-workers[92] found that dopants can stabilize the metal oxide by changing their reducibility. Trivalent dopants (Al^{3+}, Ga^{3+}) increased the conductivity of the support and activity in reverse water–gas shift and methanol synthesis, whereas divalent Mg^{2+} lowered the activity.

Surface modification. We distinguish two types of surface modification: introduction of functional groups and (complete) coating of the surface with another phase, up to the point that the surface properties are completely dictated by the coating material.

Oxygen- or nitrogen-containing functional groups are often introduced on to carbon supports as a way to regulate MSI. The basic concept is that these functionalities act as anchoring sites for the metal NPs. However, these functional groups provide more than just anchoring sites as was recognized by two groups working on the surface functionalization of CNT as support for Co catalysts during Fischer–Tropsch synthesis[93–95]. Eschemann and co-workers[95] reported substantially higher TOF for Co supported on pristine carbon nanotubes that compared with surface-oxidized CNT. The authors proposed an increased fraction of more active hexagonal close-packed Co phase on pristine CNT as the cause of these differences. This hypothesis is strengthened by looking at earlier literature, as Co was previously shown to form on a hexagonal close-packed phase on graphite (0001) (ref. [96]). In addition, several other studies showed that the role of functional groups was not limited to the anchoring of NPs during the hydrogenation[97,98] and oxidation[99] of organic compounds. Charge transfer between the functionalized support and noble metal nanoparticles substantially altered catalytic performance (Fig. 3b).

Metal oxides can also be functionalized to facilitate metal NP binding using, for example, amine or thiol groups to anchor metal NPs to a support. These functional groups can affect the activity and selectivity of catalysts supported on irreducible oxides[100,101], but this is not very common. Often the functional groups do not change the intrinsic activity of the catalysts, but rather facilitate binding to the support and can impart greater stability to the catalysts[102].

Surface coating can be applied to the support via precursor decomposition (glucose, organometallic precursors, and so on) or atomic-layer deposition. For example, coating the surface of a nanostructured In_2O_3 with carbon made this support more suitable for photocatalytic CO_2 reduction using Pt as the metal[103]. The Pt NPs were the catalytically active sites and the carbon increased the absorption of visible light through lowering of the bandgap, lowered electron-hole recombination, suppressed H_2 production from protons, and facilitated CO_2 adsorption. Through all these support functions, the production rate of CO increased from 27 to 127 $\mu mol_{CO}\ h^{-1}$, and the production of methane increased from 4 to 28 $\mu mol_{CH4}\ h^{-1}$. It should be noted that (electronic) interactions between In_2O_3 and C were present, so the composite material displayed the combined properties of both materials.

Prieto and co-workers utilized coatings to isolate the intrinsic properties of different metal oxide supports from other factors such as support morphology, and verified the effect of these properties on the performance of Ru-promoted Co catalysts[104]. The authors found a correlation between the Lewis acidity of the metal oxide surface layer and the catalytic activity and selectivity in the Fischer–Tropsch synthesis (Fig. 3c). These studies show that a surface layer can be applied to effectively replace the surface properties of the original support with that of the coating.

Metal nanoparticles

The second category of MSI tuning focusses mainly on the metal NPs. Of the three stages for MSI tuning (support, metal NP, treatment),

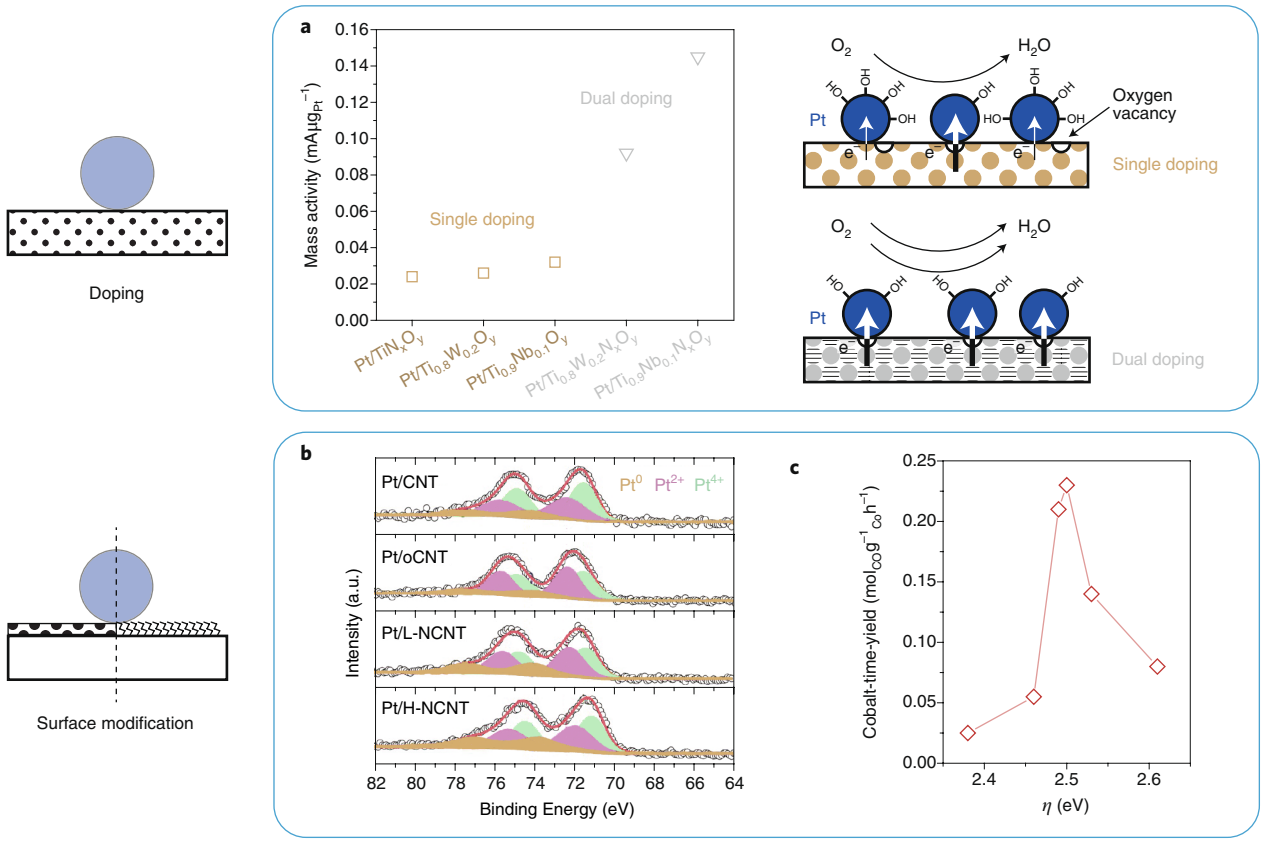

Fig. 3 | MSI tuning strategies based on doping and surface modification of the support. a, Chart comparing the electrochemical performance in the oxygen reduction reaction of Pt on various single- and dual-doped titania supports and schematic representation of the degree of charge transfer from the support to the Pt NPs depending on the kind of doping, as depicted by the thickness of the arrows. Adapted from ref. [87], Springer Nature Ltd. **b**, XPS spectra of Pt 4*f* for Pt supported on carbon nanotubes (CNT) with various pre-treatments: pristine (Pt/CNT), oxidized (Pt/oCNT), ammonia treated (Pt/L-NCNT) or high nitrogen content (Pt/H-NCNT). The spectra show changes in the oxidation state of Pt depending on the CNT surface modification. Adapted from ref. [98], American Chemical Society. **c**, Cobalt-normalized activities at pseudo-steady state for the Fischer–Tropsch synthesis reaction as a function of the acid–base character of the metal oxide surface layer inferred from the UV–vis band shift of a probe molecule (η) due to charge transfer. Adapted from ref. [104], American Chemical Society.

this is least reported, yet it does provide interesting opportunities. In this section, we will discuss recent examples of how modification of the size or composition of the nanoparticles affects MSI and hence catalytic performance.

Size. MSI can have a strong influence on the size of metal NPs, and can affect the evolution of clusters and single atoms during catalysis. For more information, we refer to a recent review for a detailed discussion on this specific topic[105]. Focussing on metal NPs, the vast majority of literature on MSI tuning deals with NPs of less than 5 nm. This is probably because the effect of the support on the metal NPs is attenuated for larger NPs because of the reduced impact of charge transfer and relatively reduced metallic surface area in intimate contact with the support, that is, fewer interface sites. NP size has the most profound influence on purely electronic MSI effects, which are short range, as Lykhach and co-workers[106] showed for 1–1.5 nm Pt NPs with a partial positive charge of 0.11 per Pt atom in the Pt/CeO_2 catalyst (Fig. 4a). They observed, using resonant photoemission spectroscopy on 2D model systems, that the partial positive charge per Pt atom decayed for larger particles. Furthermore, the overall charge transfer was limited by the support (17 % surface Ce^{3+} seems the limit for CeO_2 reduction). The need for small NPs to induce effective electronic MSI is also reflected in literature, where most reports on catalytic performance relate to particles smaller than 5 nm (see Discussion). Conversely, this also means that it is unlikely that electronic MSI plays a significant role in large (>2 nm) NPs, unless the NPs are encapsulated by the support, in which case charge transfer could still occur to all surface sites.

Guo and co-workers[107] investigated the effect of Ru NP size on the performance of Ru/CeO_2 in CO_2 hydrogenation varying between single atoms, 1 nm clusters and 4 nm NP. With increasing NP size, the electronic MSI interaction decreased, which facilitated CO_2 activation and increased reactivity (Fig. 4b). At the same time, hydrogen spillover increased with NP size, hindering H_2O removal and decreasing activity. Competition between both effects makes the 1 nm clusters (intermediate size) the most active system with a TOF about 50 % higher than single atoms and one order of magnitude higher than NPs. Interestingly, the selectivity to CH_4 was 100 % for all sizes. This is in contradiction to a recent report by Yan and co-workers[108], who observed a Ru NP size-dependent selectivity in CO_2 hydrogenation on γ-Al_2O_3. CO formation via reverse WGS was favoured for Ru clusters, while the selectivity shifted to CH_4 for larger NPs. One possible explanation for the different observations could be the nature of the supports that were employed (CeO_2 and γ-Al_2O_3), because the support was involved in the reaction in both cases. Notably, in Ru/ γ-Al_2O_3, the interface oxygen (Ru-O-Al) was shown via isotope labelling to exchange oxygen atoms with CO_2 during the reaction.

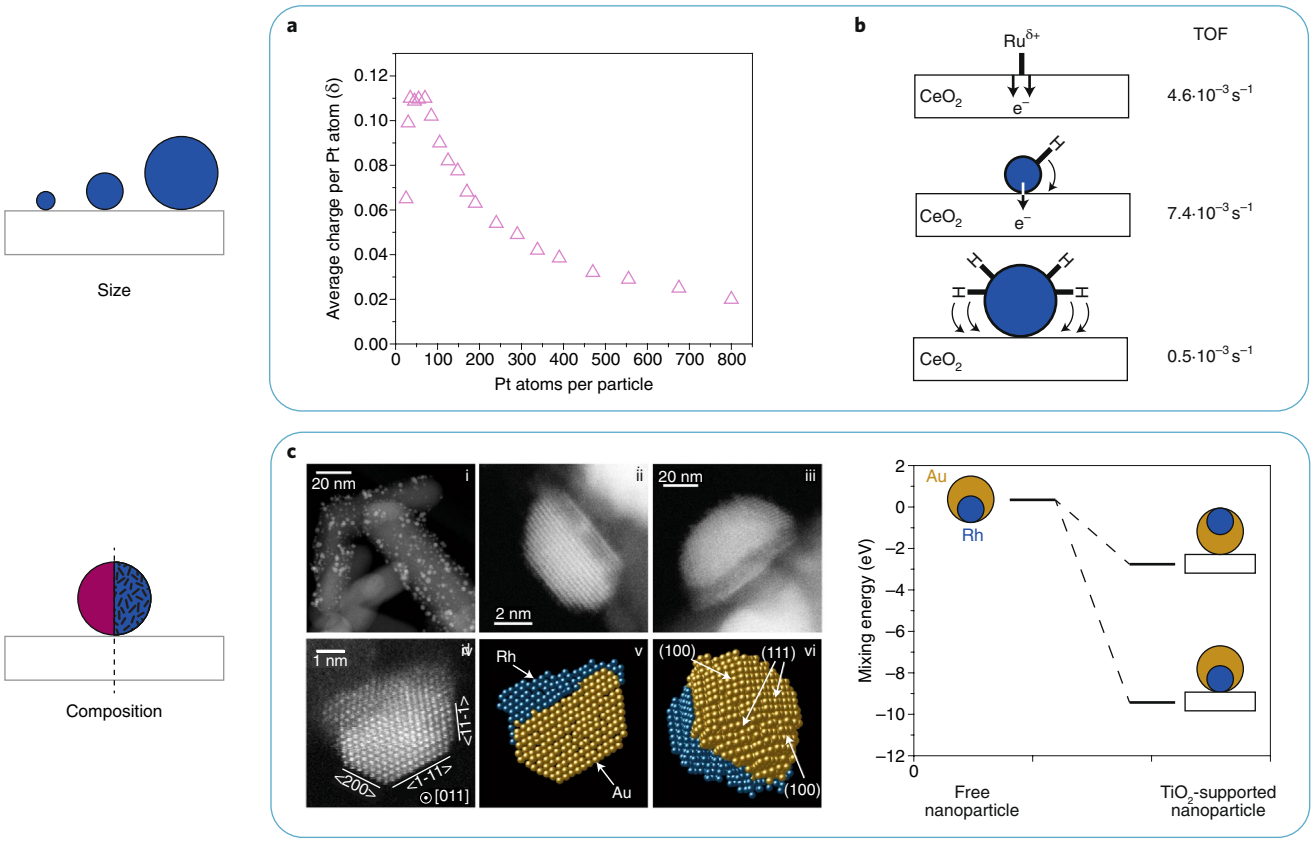

Fig. 4 | MSI tuning strategies involving alterations to the metal nanoparticle size or composition. a, Average charge per Pt atom to the ceria support as a function of the Pt particle size. Adapted from ref. [106], Springer Nature Ltd. **b**, Schematic representation of the balance between charge transfer and H-spillover for Ru of different sizes (atoms, 1 nm nanoclusters and 4 nm nanoparticles) supported on ceria and its effect on the TOF in CO_2 methanation. Adapted from ref. [107], American Chemical Society. **c**, HAADF images and model reconstruction showing Rh segregation to the TiO_2 support for a reduced AuRh/TiO_2 sample and the energy scheme for two binding configurations of AuRh clusters to TiO_2 derived from DFT. Calculations point to Rh segregation to the support as the most favourable configuration. Adapted and reproduced from ref. [110], Springer Nature Ltd.

Composition. The metal distribution in a NP depends, to a large extent, on the strength of the bonds between the metal atoms and the support. Theoretical calculations[109] on Au-Rh and Pd-Ir nanoparticles supported on titania showed that the surface binding strength of Rh or Ir atoms to TiO_2(110) is greater than that of Pd or Au to the support, due to stronger Rh-O or Ir-O interactions than Au-O or Pd-O. Therefore, Rh or Ir segregated towards TiO_2. This has been experimentally observed for Au-Rh nanoparticles supported on titania nanorods[110] (Fig. 4c), and employed for tetralin hydrogenation in the presence of H_2S (ref. [111]). The Au/Rh/TiO_2 stacking configuration had a detrimental effect on the initial hydrogenation activity. Eventually, Au/Rh/TiO_2 was more stable due to the stabilizing effect of gold against H_2S poisoning of Rh. Likewise, a segregation of iridium from Au-Ir nanoparticles towards TiO_2 has been experimentally observed, resulting in higher resistance towards sintering than Au/TiO_2 during thermal treatments[112].

For Au-Cu on Al_2O_3 and SiO_2, the NPs de-alloyed under oxidizing conditions on both supports to form Au NPs and a CuO_x phase. However, on Al_2O_3, CuO_x formed separate patches on the support, which prevented the creation of active Au-CuO_x interfacial sites present on SiO_2 (ref. [113]). Consequently, Au-CuO/SiO_2 approached 100 % CO conversion while Au-CuO/Al_2O_3 converted 11 % of the CO at 150 °C.

Seemala and co-workers[114] studied Cu-Ni nanoparticles supported on either θ-alumina or titania and observed TiO_2-induced metal segregation upon reduction using H_2, during which Cu enriched the NP surface, while Ni segregated to the NP-support interface. This arrangement was explained by a stronger interaction between nickel and titania, than copper and titania. The Cu-Ni/TiO_2 catalyst showed high activity in furfural hydrodeoxygenation, high selectivity to methyl furan and good recyclability, outperforming the Cu-Ni supported on alumina, and the titania-supported monometallic catalysts. A similar phenomenon was observed in the case of Ni-Pt supported on mesoporous silica (SBA-15)[115]. Here, a strong nickel-support interaction, most likely generated during metal precursor deposition on silica at basic conditions, led to the formation of a Pt-rich (Pt_3Ni) intermetallic compound, thus favouring the formation of active Pt-Ni bonds, rather than Ni-Ni bonds. This, in turn, increased the selectivity of CO_2 reduction to CO instead of CH_4, as the latter product is typical for Ni-based catalysts.

Divins and co-workers[116] showed that using ceria as a support influenced the oxidation state and metal arrangement of Rh-Pd nanoparticles under different atmospheres using NAP-XPS at 0.05 mbar. On reduction at 573 K, Rh-Pd/CeO_2 and non-supported Rh-Pd nanoparticles showed segregation of Pd to the surface. However, at conditions close to ethanol steam reforming, the metals in the non-supported nanoparticles re-arranged back to a uniform distribution, whereas the CeO_2-supported ones maintained the Pd-rich surface. Because the Rh-CeO_2 interaction was stronger, the core-shell structure was maintained. Furthermore, the CeO_2-supported nanoparticles presented higher oxidation states, especially at the outermost layers, due to H_2O activation at the CeO_2 surface. The high H_2 selectivity of the supported catalyst, compared

to the non-supported nanoparticles, was derived from promotion of WGS and methane steam reforming.

Gubó and co-workers[117] showed that an increase of the relative Au concentration in Au-Pd nanoparticles supported on rutile TiO_2 prevented the encapsulation of the nanoparticles by TiO_x. The nanoparticles formed a bimetallic core with an Au enriched shell and became less prone to SMSI due to the lower surface free energy of Au.

Organic ligands coordinated to the surface of metal NPs can affect MSI, for example, by acting as a carbon-precursor. Zhan and co-workers[118] placed pre-formed Au colloids, capped with oleylamine ligands, on TiO_2. The ligands were decomposed using an N_2 treatment to form a carbon shell, which protected Au NPs from sintering. The higher overall CO oxidation activity of the N_2-treated sample was ascribed to smaller NP size. Gao and colleagues[119] co-impregnated a nickel precursor and ligands on SiO_2 and obtained different NP sizes and stability during dry reforming, depending on the ligands (oleic acid, oleylamine or a mixture of both). The smaller NP size led to doubling of the CH_4 conversion, while the surface-specific activity remained unchanged (~2.5 s^{-1}).

Treatments

We define treatments as any action to modify MSI that is performed on the metal-support composite material prior to catalysis. This has mainly been investigated in the context of tuning the MSI of metals with reducible supports, that is, SMSI.

Thermal treatment. Tang and co-workers investigated MSI for various group 11 metals on TiO_2 and for Au supported on various reducible oxidic supports[120]. They observed that metal NP overgrowth under reducing conditions started at 200 °C and was most pronounced at 400–500 °C. The overgrowth blocked the accessible metallic surface area and thereby quenched the reactivity for CO oxidation, in line with earlier literature on group 8–10 metals on reducible oxides. Furthermore, a simultaneous charge transfer from the support to Au was observed by XPS, resulting in an electron rich Au phase. These effects could be reversed and the reactivity could be restored by an oxidative treatment at 400 °C. Interestingly, the same authors also observed similar effects for Au NPs supported on a phosphate hydroxyapatite, yet with the reverse response to oxidizing and reducing conditions[121]; now oxidation at 300 °C and higher resulted in the support encapsulating the Au NPs and lowering the CO oxidation activity, which could be reversed by a reductive treatment at 500 °C. It was recently suggested that loss of OH groups at high temperature gave rise to this type of interaction and the phenomenon was also observed on group 10 metals supported on ZnO-nanorods[122]. Wang and co-workers[123] even avoided the necessity for reducing or oxidising atmospheres altogether by exploiting the thermally induced transition of a layered double-hydroxide to the corresponding oxide in an inert atmosphere, possibly also caused by loss of OH groups. This induced a similar encapsulation of Au NPs with lowered CO oxidation activity.

Changes in activity and product selectivities during CO hydrogenation using Ni/Nb_2O_5 were reported after different reduction temperatures (250–450 °C) and related to SMSI effects[124]. An intermediate reduction temperature (350 °C) showed the highest activity ($3.9x10^{-5}$ mol_{CO} g_{Ni}^{-1} s^{-1}) and C_{5+}-selectivity (55 wt%). Lower reduction temperature resulted in severe deactivation due to particle growth via nickel tetracarbonyl formation and a lower final activity ($2.2x10^{-5}$ mol_{CO} g_{Ni}^{-1} s^{-1}). On the other hand, a higher reduction temperature (450 °C) displayed stable performance but with a medium activity ($2.7x10^{-5}$ mol_{CO} g_{Ni}^{-1} s^{-1}) and a selectivity shift to shorter hydrocarbon products, probably due to blockage of active sites by NbO_x suboxides. Similarly, in the case of Ni/TiO_2 catalysts for WGS, the coverage of Ni nanoparticles by TiO_x could be tuned via reduction temperatures between 400 and 600 °C (ref. [125], Fig. 5a). The metal-support interface was maximized by starting from an NiTi-layered double-hydroxide precursor. Charge transfer to interfacial Ni, coverage of Ni NP by suboxides and the number of oxygen vacancies in TiO_x all increased with higher reduction temperature. Moderate MSI after reduction at 450 °C showed the highest catalytic activity with a TOF of 3.8 s^{-1}, about two times more active than after reduction at 400, 500 or 600 °C. The high activity was attributed to the interplay between interfacial $Ni^{\delta-}$ and oxygen vacancies. In the case of Pd/TiO_2 catalysts, the reduction temperature affected the coverage of Pd NPs by TiO_x species[48] (Fig. 5b), and the number of oxygen vacancies in Pd/TiO_2 used for formaldehyde oxidation[126]. When reduced at 450 °C, more oxygen vacancies were generated, which in turn aided O_2 activation and H_2O dissociation to form OH groups and increased the formaldehyde oxidation activity 7.5-fold. These species directly decomposed formaldehyde without the slow formation of CO as an intermediate, as observed after reduction at 300 °C.

An intermetallic nickel silicide catalyst obtained by reacting a nickel complex with silica via pyrolysis at high temperatures has been shown to be highly active for chemoselective hydrogenation of a wide variety of compounds (for example, nitroarenes, carbonyls, nitriles, N-heterocycles and unsaturated carbon–carbon bonds)[127]. The researchers found that the formation of this versatile catalyst strongly depended on the pyrolysis temperature, the nitrogen-doped carbon species from the ligand for Si–O bond reduction and the silica specific surface area. A pyrolysis temperature of 600 °C resulted in metallic nickel supported on silica and on increasing the pyrolysis temperature to 800 °C, a $Ni_{17}Si_3$ phase was observed. The most active catalyst was obtained at 1,000 °C with silicon-enriched phases $Ni_{31}Si_{12}$ and Ni_2Si. Additionally, coverage of metal nanoparticles by support suboxides generated at elevated temperatures can steer hydrogenation selectivity, as summarized before[128].

Reducing agent. The extent of MSI, and, in particular, partial support reduction to form suboxides and oxygen vacancies depend on the overall severity of the reduction treatment. In 2014, Rui and co-workers[129] reported that the SMSI state in Pt/TiO_2 could be induced at room temperature during a liquid phase reduction process using $NaBH_4$ or formaldehyde as reducing agent. The SMSI state, characterized by suppressed CO chemisorption, negatively charged Pt NPs and oxygen vacancies formation, was beneficial for toluene oxidation activity, which decreased in the order $NaBH_4$ > formaldehyde > H_2. Furthermore, the MSI effect was stronger on anatase than on rutile or P25, again highlighting the importance of the support morphology as previously discussed.

Few systematic studies focusing on the effect of the reducing agent on MSI have been published in the meantime. A recent example includes the use of reducing agents with different reduction strengths to determine the rate of Pt-precursor reduction, which in turn regulated the association of NPs to different types of N-functionalities in N-doped carbon nanotubes (see the doping section)[80]. As a second recent example, Gänzler and co-workers[130,131] showed that the CO oxidation activity of Pt NPs supported on a CeO_2/Al_2O_3 composite support strongly varied as a function of the reducing agent, following the order CO > H_2 > C_3H_6 (Fig. 5c) The effect of the reducing agent was ascribed to its ability to partially reduce the support. Additionally, MSI and catalytic performance could be further tuned by reduction-oxidation cycles (see next section).

Reduction-oxidation cycles. Reduction-oxidation (RO) cycles have been intensively investigated, mainly to regulate the metal NP size through re-dispersion, but also to affect MSI in various ways. Here, we will highlight several possibilities of RO for MSI tuning that were recently published.

Besides different reducing agents, Gänzler and co-workers[130,131] applied RO cycles on a CO oxidation catalyst consisting of $Pt/CeO_2/Al_2O_3$ in order to control both the Pt NP size and oxidation state,

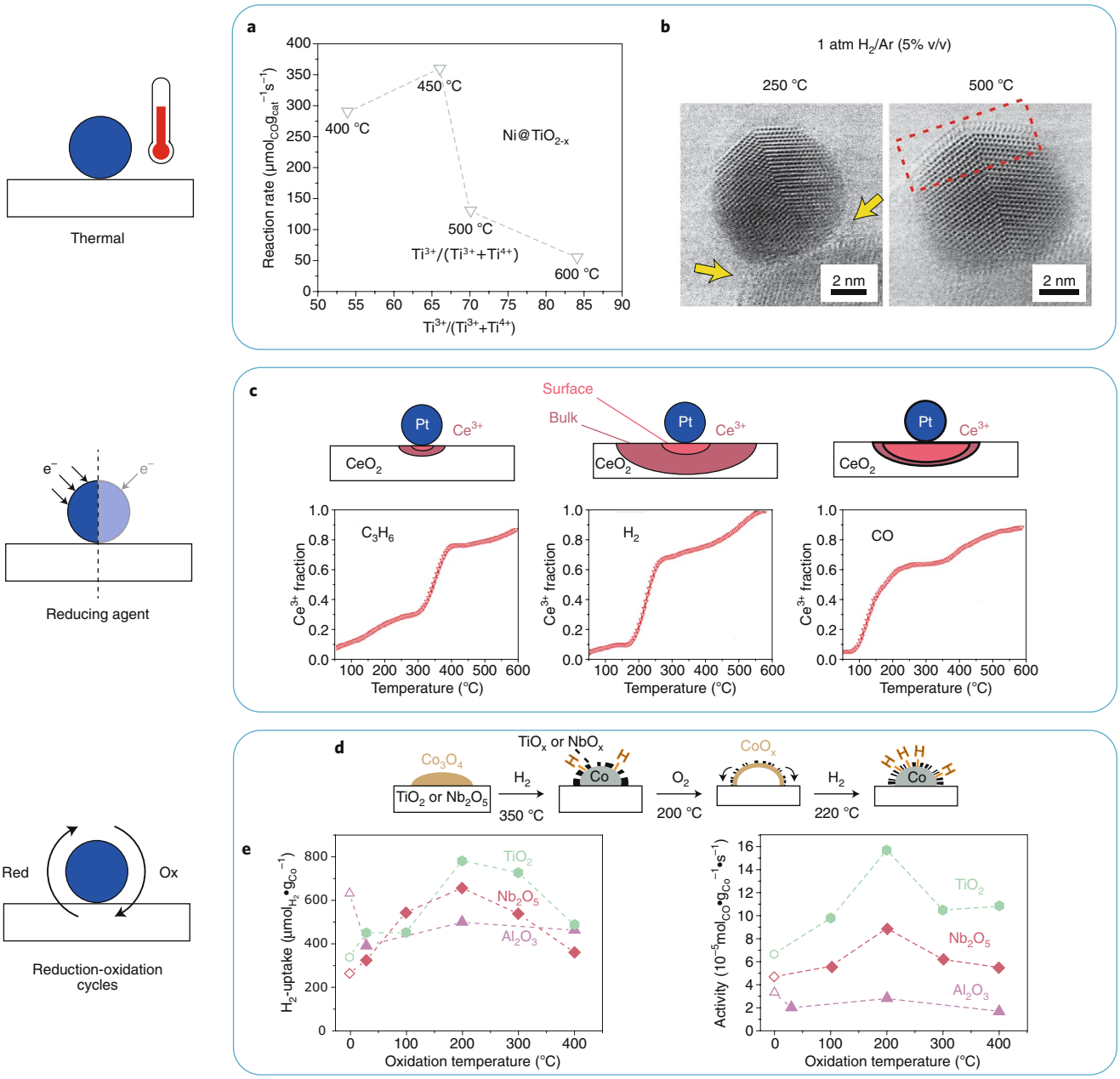

Fig. 5 | MSI tuning strategies involving treatments of supported metal catalysts based on temperature, reducing agent or reduction-oxidation cycles. **a**, The influence of reduction temperature of Ni@TiO$_x$ on the Ti^{3+} to Ti^{4+} ratio and WGS reaction rate. Adapted from ref. [125], American Chemical Society. **b**, In-situ observation of a TiO$_x$ overlayer on a Pd NP under reducing conditions at 5 vol.% H$_2$ in Ar, 1 bar, 250 and 500 °C. Reproduced from ref. [48], American Chemical Society. **c**, Support reduction using different reducing agents (C$_3$H$_6$, H$_2$ or CO) for PtO$_x$ on ceria in temperature-programmed experiments, as deduced from the fraction of Ce^{3+} obtained by Ce L3-edge XANES spectra. Adapted from ref. [131], American Chemical Society. **d**, Schematic representation of a reduction-oxidation-reduction (ROR) treatment of cobalt supported on reducible supports Reproduced from ref. [133], Springer Nature Ltd. **e**, The effect of different oxidation (O) temperatures in the ROR procedure on the hydrogen uptake in chemisorption experiments and Fischer–Tropsch synthesis activity of Co/TiO$_2$ (green hexagons), Co/Nb$_2$O$_5$ (red diamonds) and Co/Al$_2$O$_3$ (violet triangles). Singly reduced samples are indicated by open symbols. Adapted from ref. [133], Springer Nature Ltd.

which in turn affected the reduction of CeO$_2$ support. Metallic Pt NPs were necessary to reduce CeO$_2$ at low temperature and the support had a crucial role in CO oxidation, as discussed before. 1.4 nm Pt NPs were identified as the optimal size, because at this size most interfacial sites were available while maintaining the Pt NPs in the active metallic state. Further RO cycles induced Pt NP growth and reduced the CO oxidation activity

Alternatively, Freakley and co-workers[132] employed the reduction step of an RO cycle on a Pd-Sn/TiO$_2$ catalyst to selectively modify small Pd NPs that otherwise gave rise to side reactions. Surprisingly, the NPs were not covered by TiO$_x$ species, but by SnO$_x$ species, as evidenced by STEM-EELS and similarly with a Pd-Sn system supported on irreducible SiO$_2$. The final oxidation step was necessary to generate Pd^{2+} ions on the larger NPs, which were less active for side reactions than metallic Pd. The investigated reaction was the direct synthesis of H$_2$O$_2$ from O$_2$ and H$_2$ and the selectivity is a balance between the H$_2$O$_2$ production rate (hydrogenation of O$_2$) and H$_2$O$_2$ decomposition rate. By covering the small NPs and having a

Pd^{2+} containing surface on the larger NPs, the H_2O_2 decomposition was almost completely suppressed, resulting in hydrogen selectivities towards H_2O_2 of 95 %.

It is well established that the SMSI state is typically generated under reducing conditions, and that the SMSI state can be reversed by an oxidative treatment[48]. In an earlier publication[133], we applied this principle to enhance the FT activity of Co/TiO_2 and Co/Nb_2O_5 catalysts via a reduction-oxidation-reduction (ROR) process (Fig. 5d). The first reduction at 350 °C fully reduced the cobalt oxide to metallic cobalt and simultaneously induced the SMSI state. Oxidation at 200 °C modified the suboxides, but did not oxidize the cobalt fully to Co_3O_4. Consequently, the second reduction could be performed at 220 °C only, which resulted in less suboxide coverage and hence twice the accessible metallic surface area, as compared to the samples reduced at 350 °C (Fig. 5e). The FT activity increased proportionally to the metallic surface area, implying that the number of active sites increased and that the TOF and thus the nature of the active sites remained unchanged.

Overlayer deposition. As-prepared catalysts containing NPs on a support can be covered with an overlayer of another compound and its most basic function is to stabilize the NPs via immobilization, as was the case for a carbon (ref. [134]) and SiO_2 (ref. [135]) overlayer. In addition, in a 2D model study, a Pt(111) surface was covered with a thin layer of TiO_x to mimic an SMSI state[136]. Compared to the clean Pt(111) surface, the TiO_x species increased CO oxidation activity and the effect was assigned to the formation of interfacial perimeter sites. Furthermore, Weng and co-workers[137] deposited SiO_2 over Pt/Al_2O_3 and observed the formation of Brønsted acid Si-O-Al sites. The SiO_2 overlayer decreased activity in cinnamaldehyde hydrogenation, possibly via site blockage by SiO_2, while at the same time, selectivity towards cinnamyl alcohol increased from 25–30 % to 85 %.

Overlayers can also be applied to create specific interfacial sites, such as $Cu\text{-}ZrO_2$ in a Cu/SiO_2 catalyst[138]. These interface sites enhanced the intrinsic activity for ethyl acetate formation from ethanol and for methanol synthesis from CO_2 by one order of magnitude. Furthermore, Moon and co-workers[139] applied an overlayer of various reducible oxides to a Pt/SiO_2 catalyst and investigated its effect on CO oxidation. The activity followed the order $TiO_2 > CeO_2 > Pt/SiO_2 > Ta_2O_5 \approx Nb_2O_5$ and the increased activity was mainly ascribed to the formation of interfacial perimeter sites between Pt and the TiO_2 or CeO_2 overlayer. In addition, the overlayer made the catalyst more resistant towards sintering of Pt NP at elevated temperature.

Yang and co-workers[140] prepared Rh/SiO_2 catalysts covered with TiO_2 or Al_2O_3 and applied these for CO hydrogenation. The Al_2O_3 overlayer decreased the activity through site blockage. The TiO_2 overlayer, on the other hand, increased the intrinsic activity and selectivity towards C_{5+} alkanes and alkenes, while the selectivity towards higher alcohols remained unchanged. Its catalytic performance was similar to that of Rh NPs on TiO_2-coated SiO_2, showing either that coverage of the NPs themselves was irrelevant for catalysis, or that the system was dynamic and reached the same (SMSI) state during catalysis. The latter option can be rationalized considering that overlayer deposition can be used to create artificial support suboxide coverage on NPs, thereby mimicking an SMSI state[141].

Treatment of Au/TiO_2 with $TiCl_3$ at room temperature resulted in the formation of a TiO_x overlayer on Au, similar to SMSI. The TiO_x overlayer increased the activity of the catalyst for CO oxidation (0.68 versus 0.26 $mol_{CO}\ mol_{Au}^{-1}\ s^{-1}$) and brought about stability to the gold nanoparticles. The $Au\text{-}TiO_x$ interface was identified as the active site for oxygen activation, most likely due to oxygen vacancies, which were then regenerated after reaction with CO. The suboxides, however, also donated electrons to Au resulting in $Au^{\delta-}$ and decreasing CO adsorption. An oxidative pre-treatment increased the activity of the catalyst by removing the excess electrons in Au, enhancing CO adsorption[142].

Copper phyllosilicates have been employed as precursor for the formation of silica-supported metal nanoparticles on reduction in H_2, leading to high Cu loadings (~40–50 wt%) with uniform distribution and particle size. The role of the generated $Cu\text{-}SiO_2$ interface in these materials has been exploited, for example, in the decomposition of methanol to hydrogen and dimethoxymethane in the liquid phase[143], where Cu^+ and Cu-O-Si moieties were necessary for the activity and high selectivity of the catalyst. The copper-silica interface ($Cu\text{-}O\text{-}SiO_x$) was recently further optimized by use of a mesoporous silica layer coating the copper phyllosilicate prior H_2 activation[144] (Fig. 6a). In ester hydrogenation, the bare Cu/SiO_2 obtained from copper phyllosilicate gave a TOF of $6.4x10^{-3}\ s^{-1}$ and a selectivity to ethylene glycol of 23 %, whereas the performance of Cu/SiO_2 with a mesoporous silica layer increased with a TOF of $11.4x10^{-3}\ s^{-1}$ and a selectivity to ethylene glycol of 96 %. The $Cu\text{-}O\text{-}SiO_x$ interface was shown to stabilize the transition state of the ester (in this case dimethyl oxalate) and to activate H_2 in a heterolytic way, forming $Cu\text{–}H^{\delta-}$ and $SiO\text{–}H^{\delta+}$, as previously discussed for H_2 activation with nanosized non-reducible supports.

Adsorbate-mediated MSI. MSI can be tuned by adsorbing specific compounds prior to inducing the MSI state. So far, this strategy has been limited to reducible supports, because the adsorbates mainly affect the coverage of the metal NPs by support suboxides. Matsubu and co-workers[145] recently reported this strategy for the first time. They investigated Rh/TiO_2 catalysts for CO_2 hydrogenation and found that treatment in a 20 % CO_2, 2 % H_2 and 78 % He atmosphere at 250 °C caused the formation of HCO_x adsorbates on the Rh NPs. In the untreated Rh/TiO_2 sample, a crystalline SMSI overlayer, which contained Ti^{3+}-ions, formed during reduction at 550 °C, whereas the adsorbate-mediated SMSI state, induced at only 250 °C, led to an amorphous overlayer containing both Ti^{3+}- and Ti^{4+}-ions (Fig. 6b). In the adsorbate-mediated case, the support suboxides, as well as the adsorbates, can interact with the active sites. By covering the Rh NPs with an adsorbate-mediated SMSI overlayer, which was more stable under reaction conditions, it was possible to steer the catalyst selectivity from mainly CH_4-producing (on Rh NPs) to mainly CO-producing (on single Rh atoms). Rh NPs were thus more affected by the adsorbate-mediated SMSI overlayer than the single Rh atoms.

Interestingly, a similar 20 % CO_2/2 % H_2 pre-treatment was used by Wang and co-workers[146] for Cu/CeO_2 catalysts for WGS. However, they mainly used the adsorbate-mediated SMSI strategy to prevent sintering of the Cu NPs and the effect on intrinsic activity was modest, although also some charge transfer from the support to the Cu NPs was inferred from XPS. This shows that the effect of such a treatment is highly dependent on the interplay between metal, support and reaction.

Discussion

We analysed the literature to quantify the enhancement of catalytic performance that was achieved in recent years through MSI modifications. We limited the analysis largely to C_1 chemistry, that is, catalytic reactions involving CO, CH_4, CO_2 or methanol as the main reactant. The performance of tuned catalysts was benchmarked against a reference catalyst reported in the same paper and therefore investigated under the same conditions. Consequently, an enhancement factor for the tuned catalyst over the reference one was obtained. This approach provides a measure for the efficiency of the various MSI tuning strategies and facilitates comparison between different papers reporting a wide variety of reactions, conditions and units.

The rate of formation (productivity) of desirable products, that is, the product of total activity and selectivity, was taken as a

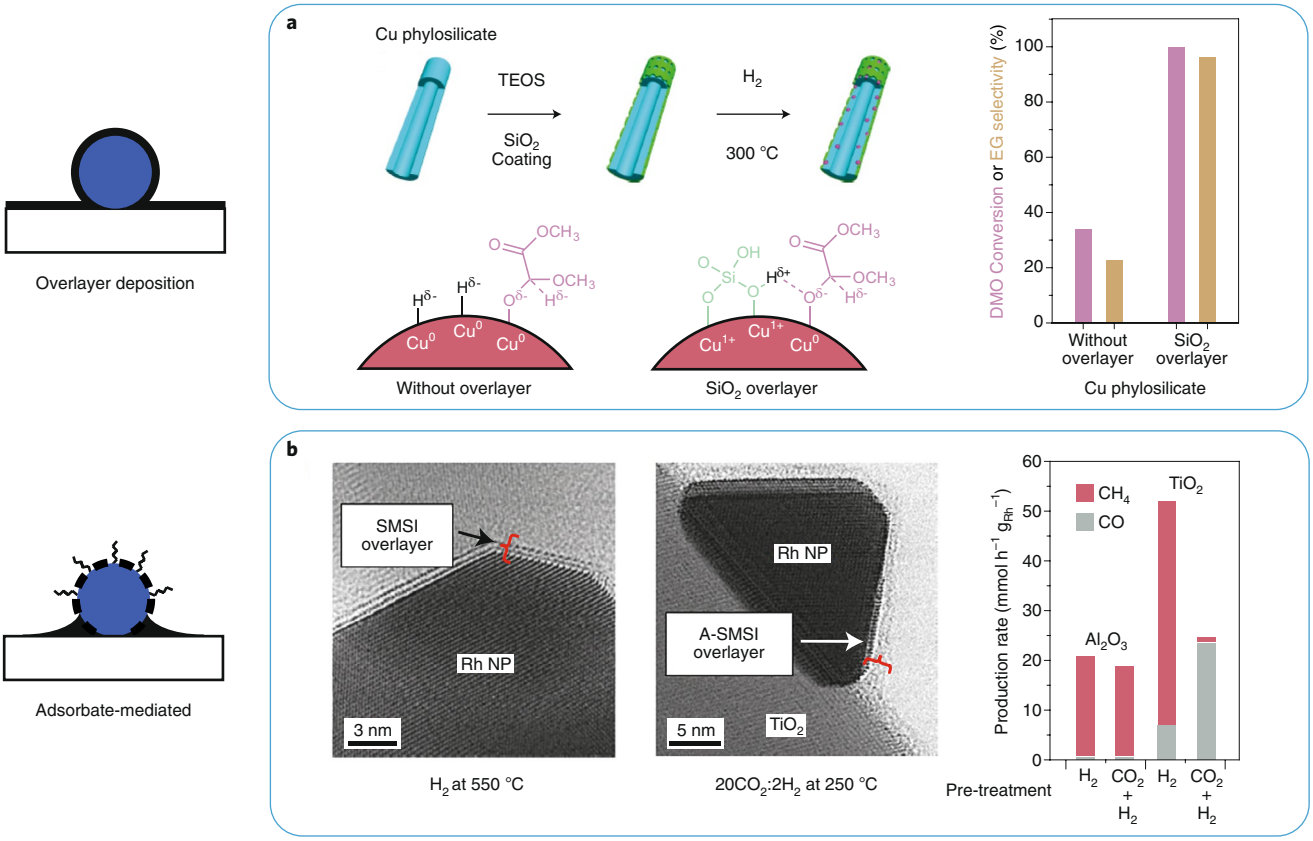

Fig. 6 | MSI tuning strategies involving overlayer deposition and adsorbate-mediated treatments of supported metal catalysts. a, Schematic representation of the effect of a silica overlayer on a copper phyllosilicate-based catalyst and the activation of dimethyl oxalate (DMO). The chart shows DMO conversion and ethylene glycol (EG) selectivity for the catalyst with and without silica overlayer. Adapted from ref. [144], Springer Nature Ltd. **b**, In-situ STEM observation of SMSI in Rh/TiO_2 after a treatment in H_2 at 550 °C which induced a TiO_x bilayer (SMSI overlayer) and after treatment in $20CO_2{:}2H_2$ at 250 °C which induced an amorphous TiO_x overlayer (A-SMSI overlayer). Production rates of CH_4 (red) and CO (grey) are shown on the chart for Rh supported on alumina or titania after H_2 or $20CO_2{:}2H_2$ treatments. Adapted from ref. [145], Springer Nature Ltd.

measure for catalytic performance. Productivity was used because this shows the combined effect of activity and selectivity changes and hence provides a more complete picture of the effect of MSI tuning than either parameter alone. Turnover frequencies or specific activities were preferred over conversions as activity descriptors, because these provide more information about intrinsic catalytic activities. Furthermore, selectivities are not relevant for certain reactions such as CO oxidation reactions. For these systems, 100% selectivity is assumed and productivity enhancement is essentially determined by activity differences. All analysed catalytic data and references can be found in Supplementary Table 1.

Figure 7a shows the productivity enhancement as a function of the different MSI tuning methods. Relative productivity enhancements up to a factor of ~15 have been obtained using various tuning methods, irrespective of which catalyst component is altered. Support modifications were effective in altering all MSI phenomena with a substantial increase of the corresponding productivity. Particularly, selection of a certain support composition[113] or adding dopants to the support[85] strongly improved the performance due to changes in the overall catalyst chemical composition. Treatments on the as-synthetized catalysts to tune the MSI have also proven beneficial to enhance their performance, and most efforts have focussed on modifying the SMSI effect from which induction of this phenomenon on Au nanoparticles by thermal treatment[120], and use of overlayer deposition of transition metal oxides[139,140] has led to significant catalytic enhancement. Reports involving strategies based on NP modifications to affect MSI were fewer, however an approach leading to substantially increased performance involved changing NP size, which in turn improved the interfacial contribution for CO_2 hydrogenation of a Ru/CeO_2 catalyst[107].

For the enhancement of selectivity, the largest increase was reported for a treatment to modify MSI in catalysts for CO_2 hydrogenation (78%), where preferential blockage of small Rh NPs or single atoms leads to a strong shift in selectivity from CH_4 towards CO (ref. [145]). However, the strong increase in selectivity was accompanied by a decrease in activity, leading to a productivity enhancement factor of 3.2. Besides this example, selectivity increases of 20–30 % are occasionally reported for various reactions. Furthermore, CO oxidation and reduction reactions were investigated most; 22 studies focused on CO oxidation and 11 on CO reduction reactions out of 50 papers analysed.

The enhancement of productivity can be correlated with metal particle size of the catalyst after MSI tuning (Fig. 7b, dataset divided on the main MSI phenomenon that was affected). In general, the efficiency of MSI tuning rapidly decayed with increasing particle size and the highest enhancements were obtained for metal particles smaller than 4 nm through modification of any MSI phenomenon. The majority of studies focused on catalysts with particle sizes in the <4 nm size range. For metal particles that are larger than 4 nm, the gain in productivity as a result of MSI tuning is modest in most cases, although a few exceptions were reported. Furthermore, for these larger particles, SMSI was most often the dominant

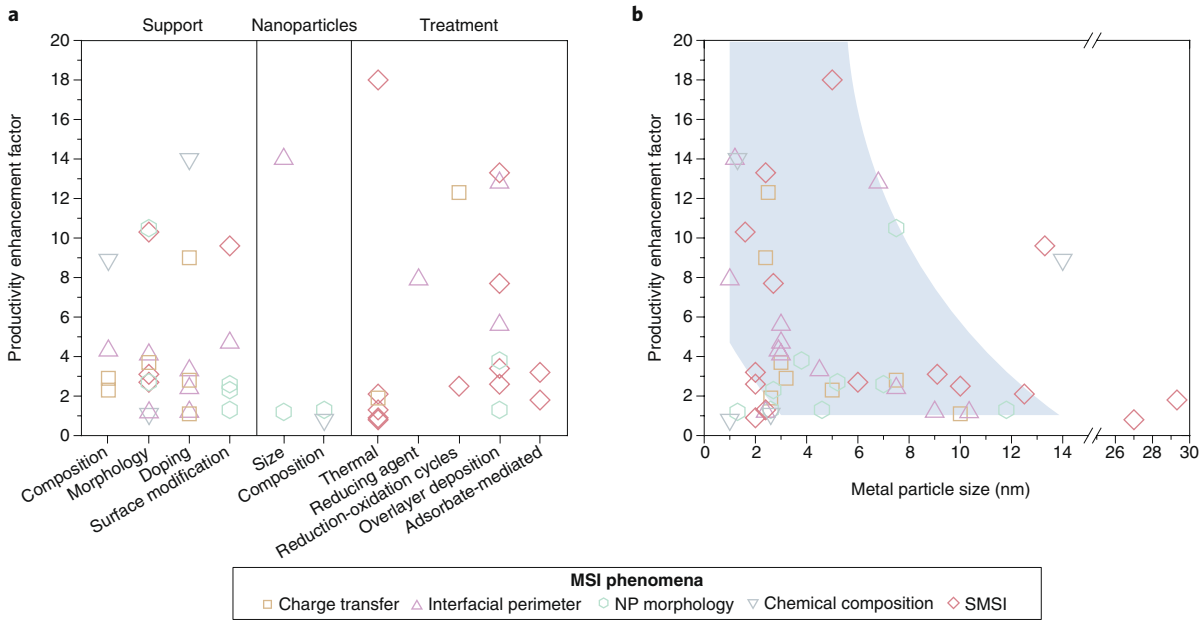

Fig. 7 | Enhancement of catalytic performance in C1 chemistry achieved through control of MSI in recent years. a, Relative differences in productivity of a desired compound for the different MSI tuning strategies grouped by general strategy (support, nanoparticle and treatment) and with different symbols indicating the main MSI phenomenon affected. Tuning strategies by modifications on the support or post-synthetic treatments have been mostly explored. **b**, Productivity enhancement factor as a function of metal particle size of the optimal catalyst, separated on the main MSI phenomenon affected by tuning. The grey-blue area is added as a guide to the eye and indicates the domain in which the NP size brought about the strongest productivity enhancement.

phenomenon, implying that SMSI is less affected by metal nanoparticle size. This can be rationalized by the support covering the NP and thus being in contact with a large fraction of the metal surface, regardless of particle size in the range described here.

When considering many types of catalysis, it became apparent that mainly late transition metals, starting from group 10, were involved when charge transfer between metal and support played a role in the catalysis. As for the supports, charge transfer with the metal required either conductive supports (for example, graphite), or semi conductive supports (reducible metal oxides), often modified by dopants to increase conductivity further. Insulators (irreducible oxides) require dopants or functionalization for charge transfer to occur on a noticeable scale[101]. This can be explained by a mismatch in band positions between insulating supports and the nanoparticles, that is, the valence band of the insulator being too low in energy to affect the electronic properties of the metal NP.

Another observation is that the work on MSI modifications for electro- and photocatalysis is limited. On one hand, this might be ascribed to early development of the role MSI in these fields of catalysis, and on the other hand, the range of applicable supports/metals might be more limited[147]. Nevertheless, we believe that the development of MSI tuning methods could be worthwhile for these applications.

Overall, MSI can improve catalytic performance roughly by one order of magnitude under industrially relevant conditions. This effect may seem modest compared to, for example, a difference of four orders of magnitude in CO hydrogenation activity that is obtained with various metals from groups 8–10 in the periodic table[148]. However, often the selection of the metal is fixed by selectivity considerations and MSI modification is one of the few effective tools for designing and enhancing catalyst performance. In addition, these results show that supports are more than merely an inert structural matrix and that their chemical properties can be applied to substantially improve catalytic performance.

Received: 17 May 2019; Accepted: 4 September 2019;
Published online: 4 November 2019

References

1. Anderson, J.A. & García, M.F. *Supported Metals in Catalysis: Catalytic Science Series* Vol. 5 (Imperial College Press, 2005).
2. Roldan Cuenya, B. Synthesis and catalytic properties of metal nanoparticles: size, shape, support, composition, and oxidation state effects. *Thin Solid Films* **518**, 3127–3150 (2010).
3. Zečević, J., Vanbutsele, G., de Jong, K. P. & Martens, J. A. Nanoscale intimacy in bifunctional catalysts for selective conversion of hydrocarbons. *Nature* **528**, 245–248 (2015).
4. Arnal, P. M., Comotti, M. & Schüth, F. High-temperature-stable catalysts by hollow sphere encapsulation. *Angew. Chem. Int. Ed.* **45**, 8224–8227 (2006).
5. Pacchioni, G. & Freund, H.-J. Controlling the charge state of supported nanoparticles in catalysis: lessons from model systems. *Chem. Soc. Rev.* **47**, 8474–8502 (2018).
6. Farmer, Ja & Campbell, C. T. Ceria maintains smaller metal catalyst particles by strong metal-support bonding. *Science* **329**, 933–936 (2010).
7. Ahmadi, M., Mistry, H. & Roldan Cuenya, B. Tailoring the catalytic properties of metal nanoparticles via support interactions. *J. Phys. Chem. Lett.* **7**, 3519–3533 (2016).
8. Ro, I., Resasco, J. & Christopher, P. Approaches for understanding and controlling interfacial effects in oxide-supported metal catalysts. *ACS Catal.* **8**, 7368–7387 (2018).
9. Pan, C.-J. et al. Tuning/exploiting strong metal-support interaction (SMSI) in heterogeneous catalysis. *J. Taiwan Inst. Chem. Eng.* **74**, 154–186 (2017).
10. Fujiwara, K., Okuyama, K. & Pratsinis, S. E. Metal–support interactions in catalysts for environmental remediation. *Environ. Sci. Nano* **4**, 2076–2092 (2017).
11. Chen, M. S. & Goodman, D. W. The structure of catalytically active gold on titania. *Science* **306**, 252–255 (2004).
12. Luches, P. et al. Nature of Ag islands and nanoparticles on the CeO_2(111) surface. *J. Phys. Chem. C.* **116**, 1122–1132 (2011).
13. Pacchioni, G. Electronic interactions and charge transfers of metal atoms and clusters on oxide surfaces. *Phys. Chem. Chem. Phys.* **15**, 1737–1757 (2013).
14. Puigdollers, A. R., Schlexer, P., Tosoni, S. & Pacchioni, G. Increasing oxide reducibility: the role of metal/oxide interfaces in the formation of oxygen vacancies. *ACS Catal.* **7**, 6493–6513 (2017).

15. Molina, L. M. & Hammer, B. Some recent theoretical advances in the understanding of the catalytic activity of Au. *Appl. Catal. A Gen.* **291**, 21–31 (2005).
16. Zhang, B. & Qin, Y. Interface tailoring of heterogeneous catalysts by atomic layer deposition. *ACS Catal.* **8**, 10064–10081 (2018).
17. Lin, X. et al. Characterizing low-coordinated atoms at the periphery of MgO-supported Au islands using scanning tunneling microscopy and electronic structure calculations. *Phys. Rev. B.* **81**, 6–9 (2010).
18. Hammer, B. Special sites at noble and late transition metal catalysts. *Top. Catal.* **37**, 3–16 (2006).
19. Farnesi Camellone, M., Negreiros Ribeiro, F., Szabová, L., Tateyama, Y. & Fabris, S. Catalytic proton dynamics at the water/solid interface of ceria-supported Pt clusters. *J. Am. Chem. Soc.* **138**, 11560–11567 (2016).
20. Toebes, M. L. et al. Support effects in hydrogenation of cinnamaldehyde over carbon nanofiber-supported platinum catalysts: kinetic modelling. *Chem. Eng. Sci.* **60**, 5682–5695 (2005).
21. Davis, S. E., Ide, M. S. & Davis, R. J. Selective oxidation of alcohols and aldehydes over supported metal nanoparticles. *Green. Chem.* **15**, 17–45 (2013).
22. Conner, W. C. & Falconer, J. L. Spillover in heterogeneous catalysis. *Chem. Rev.* **95**, 759–788 (1995).
23. Prins, R. Hydrogen spillover: facts and fiction. *Chem. Rev.* **112**, 2714–2738 (2012).
24. Takakusagi, S., Fukui, K. I., Tero, R., Asakura, K. & Iwasawa, Y. First direct visualization of spillover species emitted from Pt nanoparticles. *Langmuir* **26**, 16392–16396 (2010).
25. Karim, W. et al. Catalyst support effects on hydrogen spillover. *Nature* **541**, 68–71 (2017).
26. Roldan Cuenya, B. Metal nanoparticle catalysts beginning to shape-up. *Acc. Chem. Res.* **46**, 1682–1691 (2012).
27. Frenkel, A. I. et al. Correlating particle size and shape of supported Ru/γ-Al_2O_3 catalysts with NH_3 decomposition activity. *J. Am. Chem. Soc.* **131**, 12230–12239 (2009).
28. Henry, C. R. Morphology of supported nanoparticles. *Prog. Surf. Sci.* **80**, 92–116 (2005).
29. Hansen, P. L. et al. Atom-resolved imaging of dynamic shape changes in supported copper nanocrystals. *Science* **295**, 2053–2055 (2002).
30. Hemmingson, S. L. & Campbell, C. T. Trends in adhesion energies of metal nanoparticles on oxide surfaces: understanding support effects in catalysis and nanotechnology. *ACS Nano* **11**, 1196–1203 (2017).
31. Ahmadi, M., Behafarid, F. & Roldan Cuenya, B. Size-dependent adhesion energy of shape-selected Pd and Pt nanoparticles. *Nanoscale* **8**, 11635–11641 (2016).
32. Tanase, M. et al. Interfacial bonding stabilizes rhodium and rhodium oxide nanoparticles on layered Nb oxide and Ta oxide dupports. *J. Am. Chem. Soc.* **136**, 5687–5696 (2014).
33. Duan, M. et al. Reconstruction of supported metal nanoparticles in reaction conditions. *Angew. Chem. Int. Ed.* **57**, 6464–6469 (2018).
34. Lin, Y. et al. Adhesion and atomic structures of gold on ceria nanostructures: the role of surface structure and oxidation state of ceria rupports. *Nano Lett.* **15**, 5375–5381 (2015).
35. Pingel, T. N., Jørgensen, M., Yankovich, A. B., Grönbeck, H. & Olsson, E. Influence of atomic site-specific strain on catalytic activity of supported nanoparticles. *Nat. Commun.* **9**, 2722 (2018).
Platinum nanoparticles anchored to γ-Al_2O_3 or CeO_2 show different levels of strain, which the authors quantify and they calculate the optimal Pt NP strain pattern for CO oxidation.
36. Shibata, N. et al. Interface structures of gold nanoparticles on TiO_2 (110). *Phys. Rev. Lett.* **102**, 136105 (2009).
37. Bartholomew, C. H. Mechanisms of catalyst deactivation. *Appl. Catal. A Gen.* **212**, 17–60 (2001).
38. van Deelen, T. W., Nijhuis, J. J., Krans, N. A., Zečević, J. & de Jong, K. P. Preparation of cobalt nanocrystals supported on metal oxides to study particle growth in Fischer–Tropsch catalysts. *ACS Catal.* **8**, 10581–10589 (2018).
39. Penner, S. & Armbrüster, M. Formation of intermetallic compounds by reactive metal– support interaction: a frequently encountered phenomenon in catalysis. *ChemCatChem* **7**, 374–392 (2015).
40. Furukawa, S. & Komatsu, T. Intermetallic compounds: promising inorganic materials for well-structured and electronically modified reaction environments for efficient catalysis. *ACS Catal.* **7**, 735–765 (2017).
41. Zafeiratos, S., Piccinin, S. & Teschner, D. Alloys in catalysis: phase separation and surface segregation phenomena in response to the reactive environment. *Catal. Sci. Technol.* **2**, 1787–1801 (2012).
42. Singh, A. K. & Xu, Q. Synergistic catalysis over bimetallic alloy nanoparticles. *ChemCatChem* **5**, 652–676 (2013).
43. Ferrando, R., Jellinek, J. & Johnston, R. L. Nanoalloys: From theory to applications of alloy clusters and nanoparticles. *Chem. Rev.* **108**, 845–910 (2008).
44. Tauster, S. J., Fung, S. C. & Garten, R. L. Strong metal-support interactions: group 8 noble metals supported on titanium dioxide. *J. Am. Chem. Soc.* **100**, 170–175 (1978).
45. Tauster, S. J., Fung, S. C., Baker, R. T. & Horsley, J. A. Strong interactions in supported-metal catalysts. *Science* **211**, 1121–1125 (1981).
46. Hernández-Cristóbal, O., Arenas-Alatorre, J., Díaz, G., Bahena, D. & J. Yacamán, M. High resolution HAADF characterization of Ir/TiO_2 catalyst reduced at 500 °C: intensity profile analysis. *J. Phys. Chem. C.* **119**, 11672–11678 (2015).
47. Willinger, M. G. et al. A case of strong metal–support interactions: combining advanced microscopy and model systems to elucidate the atomic structure of interfaces. *Angew. Chem. Int. Ed.* **53**, 5998–6001 (2014).
48. Zhang, S. et al. Dynamical observation and detailed description of catalysts under strong metal–support interaction. *Nano Lett.* **16**, 4528–4534 (2016).
49. Chen, M. S. & Goodman, D. W. Interaction of Au with titania: the role of reduced Ti. *Top. Catal.* **44**, 41–47 (2007).
50. Saavedra, J., Pursell, C. J. & Chandler, B. D. CO oxidation kinetics over Au/TiO_2 and Au/Al_2O_3 catalysts: evidence for a common water-assisted mechanism. *J. Am. Chem. Soc.* **140**, 3712–3723 (2018).
51. Wang, Y., Widmann, D. & Behm, R. J. Influence of TiO_2 bulk defects on CO adsorption and CO oxidation on Au/TiO_2: electronic metal–support interactions (EMSIs) in supported Au catalysts. *ACS Catal.* **7**, 2339–2345 (2017).
52. Wang, Y. et al. The role of electronic metal-support interactions and its temperature dependence: CO adsorption and CO oxidation on Au/TiO_2 catalysts in the presence of TiO2 bulk defects. *J. Catal.* **354**, 46–60 (2017).
53. Kumar, G. et al. Evaluating differences in the active-site electronics of supported Au nanoparticle catalysts using Hammett and DFT studies. *Nat. Chem.* **10**, 268–274 (2018).
The catalytic performance of gold nanoparticles on various supports is compared using a model reaction to obtain information on the role of charge transfer between metal and support.
54. Song, H. et al. Visible-light-mediated methane activation for steam methane reforming under mild conditions: a case study of Rh/TiO_2 catalysts. *ACS Catal.* **8**, 7556–7565 (2018).
55. Sakamoto, H. et al. Hot-electron-induced highly efficient O_2 activation by Pt nanoparticles supported on Ta_2O_5 driven by visible light. *J. Am. Chem. Soc.* **137**, 9324–9332 (2015).
56. Jackson, C. et al. Electronic metal-support interaction enhanced oxygen reduction activity and stability of boron carbide supported platinum. *Nat. Commun.* **8**, 15802 (2017).
Platinum nanoparticles supported on boron carbide outperform commercial Pt/C in terms of activity and stability, which is ascribed to an electronic metal-support interaction.
57. Irvine, J. T. S. et al. Evolution of the electrochemical interface in high-temperature fuel cells and electrolysers. *Nat. Energy* **1**, 1–13 (2016).
58. Neagu, D., Tsekouras, G., Miller, D. N., Ménard, H. & Irvine, J. T. S. In situ growth of nanoparticles through control of non-stoichiometry. *Nat. Chem.* **5**, 916–923 (2013).
59. Neagu, D. et al. Nano-socketed nickel particles with enhanced coking resistance grown in situ by redox exsolution. *Nat. Commun.* **6**, 8120 (2015).
60. Gao, Y., Wang, J., Lyu, Y.-Q., Lam, K. & Ciucci, F. In situ growth of Pt_3Ni nanoparticles on an A-site deficient perovskite with enhanced activity for the oxygen reduction reaction. *J. Mater. Chem. A* **5**, 6399–6404 (2017).
61. Huang, X., Zhao, G., Wang, G. & Irvine, J. T. S. Synthesis and applications of nanoporous perovskite metal oxides. *Chem. Sci.* **9**, 3623–3637 (2018).
62. Murata, K. et al. The metal-support interaction concerning the particle size Effect of Pd/Al_2O_3 on Methane Combustion. *Angew. Chem. Int. Ed.* **56**, 15993–15997 (2017).
63. Bertella, F., Concepción, P. & Martínez, A. TiO_2 polymorph dependent SMSI effect in Co-Ru/TiO_2 catalysts and its relevance to Fischer–Tropsch synthesis. *Catal. Today* **289**, 181–191 (2017).
64. Yu, L. et al. Influence of the crystal structure of titanium oxide on the catalytic activity of Rh/TiO_2 in steam reforming of propane at low temperature. *Chem. Eur. J.* **24**, 8742–8746 (2018).
65. Bertella, F., Concepción, P. & Martínez, A. The impact of support surface area on the SMSI decoration effect and catalytic performance for Fischer-Tropsch synthesis of Co-Ru/TiO_2-anatase catalysts. *Catal. Today* **296**, 170–180 (2017).
66. Abdel-Mageed, A. M. et al. Selective CO methanation on Ru/TiO_2 Catalysts: role and influence of metal-support interactions. *ACS Catal.* **5**, 6753–6763 (2015).
67. Yoon, S. et al. Specific metal-support interactions between nanoparticle layers for catalysts with enhanced methanol oxidation activity. *ACS Catal.* **8**, 5391–5398 (2018).
68. Lin, B. et al. Effect of ceria morphology on the catalytic activity of Co/CeO_2 catalyst for ammonia synthesis. *Catal. Commun.* **101**, 15–19 (2017).

69. Ma, Z., Zhao, S., Pei, X., Xiong, X. & Hu, B. New insights into the support morphology-dependent ammonia synthesis activity of Ru/CeO_2. *catalysts. Catal. Sci. Technol.* **7**, 191–199 (2017).
70. Ha, H., Yoon, S., An, K. & Kim, H. Y. Catalytic CO oxidation over Au nanoparticles supported on CeO_2 nanocrystals: effect of the Au–CeO_2 interface. *ACS Catal.* **8**, 11491–11501 (2018).
71. Liu, M.-H., Chen, Y.-W., Lin, T.-S. & Mou, C.-Y. Defective mesocrystal ZnO-supported gold catalysts: facilitating CO oxidation via vacancy defects in ZnO. *ACS Catal.* **8**, 6862–6869 (2018).
72. Zhu, W. et al. Taming interfacial electronic properties of platinum nanoparticles on vacancy-abundant boron nitride nanosheets for enhanced catalysis. *Nat. Commun.* **8**, 15291 (2017).
73. Yan, X. et al. Nickel@Siloxene catalytic nanosheets for high-performance CO_2 methanation. *Nat. Commun.* **10**, 2608 (2019).
74. Zhang, F. et al. Tailoring the oxidation activity of Pt nanoclusters via encapsulation. *ACS Catal.* **5**, 1381–1385 (2015).
75. Li, Z. et al. Reactive metal–support interactions at moderate temperature in two-dimensional niobium-carbide-supported platinum catalysts. *Nat. Catal.* **1**, 349–355 (2018).
A Pt-Nb surface alloy with enhanced water–gas shift kinetics is generated under reaction conditions from a two-dimensional metal carbide using the concept of reactive metal-support interactions.
76. Li, Z. et al. Two-dimensional transition metal carbides as supports for tuning the chemistry of catalytic nanoparticles. *Nat. Commun.* **9**, 5258 (2018).
77. Shi, L., Li, Z., Dao, T. D., Nagao, T. & Yang, Y. A synergistic interaction between isolated Au nanoparticles and oxygen vacancies in an amorphous black TiO_2 nanoporous film: toward enhanced photoelectrochemical water splitting. *J. Mater. Chem. A* **6**, 12978–12984 (2018).
78. He, L., Weniger, F., Neumann, H. & Beller, M. Synthesis, characterization, and application of metal nanoparticles supported on nitrogen-doped carbon: catalysis beyond electrochemistry. *Angew. Chem. Int. Ed.* **55**, 12582–12594 (2016).
79. Shi, R. et al. Nitrogen-doped graphene supported copper catalysts for methanol oxidative carbonylation: enhancement of catalytic activity and stability by nitrogen species. *Carbon* **130**, 185–195 (2018).
80. Ning, X. et al. Electron transfer dependent catalysis of Pt on N-doped carbon nanotubes: effects of synthesis method on metal-support interaction. *J. Catal.* **348**, 100–109 (2017).
81. Walczak, R. et al. Template- and metal-free synthesis of nitrogen-rich nanoporous "noble" varbon materials by direct pyrolysis of a preorganized hexaazatriphenylene precursor. *Angew. Chem. Int. Ed.* **57**, 10765–10770 (2018).
82. Antonietti, M. & Oschatz, M. The concept of "noble, heteroatom-doped carbons," their directed synthesis by electronic band control of carbonization, and applications in catalysis and energy materials. *Adv. Mater.* **30**, 1706836 (2018).
83. Qin, Q., Heil, T., Antonietti, M. & Oschatz, M. Single-site gold catalysts on hierarchical N-doped porous noble carbon for enhanced electrochemical reduction of nitrogen. *Small Methods* **2**, 1800202 (2018).
Gold nanoparticles are positively charged on a C_2N noble carbon support, making them active for ammonia synthesis.
84. Theofanidis, S. A. et al. Fe-containing magnesium aluminate support for stability and carbon control during methane reforming. *ACS Catal.* **8**, 5983–5995 (2018).
85. Margossian, T. et al. Molecularly tailored nickel precursor and support yield a stable methane dry reforming catalyst with superior metal utilization. *J. Am. Chem. Soc.* **139**, 6919–6927 (2017).
86. Horlyck, J., Lewis, S., Amal, R. & Scott, J. The impact of La doping on dry reforming Ni-based catalysts loaded on FSP-alumina. *Top. Catal.* **61**, 1842–1855 (2018).
87. Hsieh, B.-J. et al. Platinum loaded on dual-doped TiO_2 as an active and durable oxygen reduction reaction catalyst. *NPG Asia Mater.* **9**, e403 (2017).
88. Tran, S. B. T., Choi, H. S., Oh, S. Y., Moon, S. Y. & Park, J. Y. Iron-doped ZnO as a support for Pt-based catalysts to improve activity and stability: enhancement of metal-support interaction by the doping effect. *RSC Adv.* **8**, 21528–21533 (2018).
89. Wang, F. et al. Enhanced catalytic performance of Ir catalysts supported on ceria-based solid solutions for methane dry reforming reaction. *Catal. Today* **281**, 295–303 (2017).
90. Tabakova, T. et al. Structure-activity relationship in water-gas shift reaction over gold catalysts supported on Y-doped ceria. *J. Rare Earths* **37**, 383–392 (2019).
91. Chen, P. et al. Experimental and theoretical understanding of nitrogen-doping-induced strong metal-support interactions in Pd/TiO_2 catalysts for nitrobenzene hydrogenation. *ACS Catal.* **7**, 1197–1206 (2017).
92. Schumann, J. et al. Promoting strong metal support interaction: doping ZnO for enhanced activity of Cu/ZnO:M (M = Al, Ga, Mg) catalysts. *ACS Catal.* **5**, 3260–3270 (2015).
93. Chernyak, S. A. et al. Effect of Co crystallinity on Co/CNT catalytic activity in CO/CO_2 hydrogenation and CO disproportionation. *Appl. Surf. Sci.* **372**, 100–107 (2016).
94. Chernyak, S. A. et al. Co catalysts supported on oxidized CNTs: evolution of structure during preparation, reduction and catalytic test in Fischer-Tropsch synthesis. *Appl. Catal. A Gen.* **523**, 221–229 (2016).
95. Eschemann, T. O. et al. Effect of support surface treatment on the synthesis, structure, and performance of Co/CNT Fischer–Tropsch catalysts. *J. Catal.* **328**, 130–138 (2015).
96. Honma, T. & Wayman, C. M. Epitaxial growth of evaporated cobalt films. *J. Appl. Phys.* **36**, 2791–2798 (1965).
97. Rao, R. G. et al. Interfacial charge distributions in carbon-supported palladium catalysts. *Nat. Commun.* **8**, 340 (2017).
The selectivity of Pd/C catalysts in cinnamaldehyde hydrogenation is regulated by functional groups on the support surface, because of electronic charge redistribution at the Pd-C interface.
98. Shi, W. et al. Enhanced chemoselective hydrogenation through tuning the interaction between Pt nanoparticles and carbon supports: insights from identical location transmission electron microscopy and X-ray photoelectron spectroscopy. *ACS Catal.* **6**, 7844–7854 (2016).
99. Donoeva, B., Masoud, N. & De Jongh, P. E. Carbon support surface effects in the gold-catalyzed oxidation of 5-hydroxymethylfurfural. *ACS Catal.* **7**, 4581–4591 (2017).
100. Celebi, M., Yurderi, M., Bulut, A., Kaya, M. & Zahmakiran, M. Palladium nanoparticles supported on amine-functionalized SiO_2 for the catalytic hexavalent chromium reduction. *Appl. Catal. B Environ.* **180**, 53–64 (2016).
101. Rodríguez-Gómez, A., Platero, F., Caballero, A. & Colón, G. Improving the direct synthesis of hydrogen peroxide from hydrogen and oxygen over Au-Pd/SBA-15 catalysts by selective functionalization. *Mol. Catal.* **445**, 142–151 (2018).
102. Van Den Berg, R. et al. Support functionalization to retard ostwald ripening in copper methanol synthesis catalysts. *ACS Catal.* **5**, 4439–4448 (2015).
103. Pan, Y.-X. et al. Photocatalytic CO_2 reduction by carbon-coated indium-oxide nanobelts. *J. Am. Chem. Soc.* **139**, 4123–4129 (2017).
104. Prieto, G. et al. Cobalt-catalyzed Fischer-Tropsch synthesis: chemical nature of the oxide support as a performance descriptor. *ACS Catal.* **5**, 3323–3335 (2015).
105. Liu, L. & Corma, A. Metal catalysts for heterogeneous catalysis: from single atoms to nanoclusters and nanoparticles. *Chem. Rev.* **118**, 4981–5079 (2018).
106. Lykhach, Y. et al. Counting electrons on supported nanoparticles. *Nat. Mater.* **15**, 284–288 (2016).
Charge donation per platinum atom in Pt/CeO_2 catalysts is quantified, showing that charge transfer is only effective at short range, with an optimum for nanoparticles consisting of 30–70 Pt atoms.
107. Guo, Y. et al. Low-temperature CO_2 methanation over CeO_2-supported Ru single atoms, nanoclusters, and nanoparticles competitively tuned by strong metal-support interactions and H-spillover effect. *ACS Catal.* **8**, 6203–6215 (2018).
108. Yan, Y. et al. Ru/Al_2O_3 catalyzed CO_2 hydrogenation: oxygen-exchange on metal-support interfaces. *J. Catal.* **367**, 194–205 (2018).
109. Demiroglu, I. et al. Modelling free and oxide-supported nanoalloy catalysts: comparison of bulk-immiscible Pd–Ir and Au–Rh systems and influence of a TiO_2 support. *Faraday Discuss.* **208**, 53–66 (2018).
110. Piccolo, L. et al. Understanding and controlling the structure and segregation behaviour of AuRh nanocatalysts. *Sci. Rep.* **6**, 1–8 (2016).
111. Konuspayeva, Z. et al. Au-Rh and Au-Pd nanocatalysts supported on rutile titania nanorods: structure and chemical stability. *Phys. Chem. Chem. Phys.* **17**, 28112–28120 (2015).
112. Han, C. W. et al. Highly stable bimetallic AuIr/TiO_2 catalyst: physical origins of the intrinsic high stability against sintering. *Nano Lett.* **15**, 8141–8147 (2015).
113. Destro, P. et al. The crucial role of the support in the transformations of bimetallic nanoparticles and catalytic performance. *ACS Catal.* **8**, 1031–1037 (2018).
114. Seemala, B., Cai, C. M., Wyman, C. E. & Christopher, P. Support induced control of surface composition in Cu-Ni/TiO_2 catalysts enables high yield co-conversion of HMF and furfural to methylated furans. *ACS Catal.* **7**, 4070–4082 (2017).
115. Liu, D. et al. Identifying dynamic structural changes of active sites in Pt–Ni bimetallic catalysts using multimodal approaches. *ACS Catal.* **8**, 4120–4131 (2018).
116. Divins, N. J., Angurell, I., Escudero, C., Pérez-Dieste, V. & Llorca, J. Influence of the support on surface rearrangements of bimetallic nanoparticles in real catalysts. *Science* **346**, 620–623 (2014).
Rh and Pd are uniformly distributed in unsupported bimetallic nanoparticles at conditions close to ethanol steam reforming, whereas

in CeO_2-supported bimetallic NP under the same conditions, Pd is enriched at the NP surface in and Rh coordinates to the support.
117. Gubó, R. et al. Variation of SMSI with the Au:Pd ratio of bimetallic nanoparticles on TiO_2(110). *Top. Catal.* **61**, 308–317 (2018).
118. Zhan, W. et al. Surfactant-assisted stabilization of Au colloids on solids for heterogeneous catalysis. *Angew. Chem. Int. Ed.* **56**, 4494–4498 (2017).
119. Gao, X., Liu, H., Hidajat, K. & Kawi, S. Anti-coking Ni/SiO_2 catalyst for dry reforming of methane: tole of oleylamine/oleic acid organic pair. *ChemCatChem* **7**, 4188–4196 (2015).
120. Tang, H. et al. Classical strong metal–support interactions between gold nanoparticles and titanium dioxide. *Sci. Adv.* **3**, e1700231 (2017).
Coverage of gold nanoparticles by TiO_2 suboxides occurs during H_2 treatment at elevated temperature and limits accessibility of the Au surface, thereby quenching CO oxidation reactivity.
121. Tang, H. et al. Strong metal-support Interactions between gold nanoparticles and nonoxides. *J. Am. Chem. Soc.* **138**, 56–59 (2016).
122. Tang, H. et al. Oxidative strong metal-support interactions (OMSI) of supported platinum-group metal catalysts. *Chem. Sci.* **9**, 6679–6684 (2018).
123. Wang, L. et al. Strong metal-support interactions achieved by hydroxide-to-oxide support transformation for preparation of sinter-resistant gold nanoparticle catalysts. *ACS Catal.* **7**, 7461–7465 (2017).
124. Hernández Mejía, C., Vogt, C., Weckhuysen, B.M. & de Jong, K.P. Stable niobia-supported nickel catalysts for the hydrogenation of carbon monoxide to hydrocarbons. *Catal. Today* https://doi.org/10.1016/j.cattod.2018.11.036 (2018).
125. Xu, M. et al. TiO_{2-x}-modified Ni nanocatalyst with tunable metal–support interaction for water–gas shift reaction. *ACS Catal.* **7**, 7600–7609 (2017).
126. Li, Y. et al. High temperature reduction dramatically promotes Pd/TiO_2 catalyst for ambient formaldehyde oxidation. *Appl. Catal. B Environ.* **217**, 560–569 (2017).
127. Ryabchuk, P. et al. Intermetallic nickel silicide nanocatalyst—a non-noble metal–based general hydrogenation catalyst. *Sci. Adv.* **4**, eaat0761 (2018).
128. Serna, P. & Corma, A. Transforming nano metal nonselective particulates into chemoselective catalysts for hydrogenation of substituted nitrobenzenes. *ACS Catal.* **5**, 7114–7121 (2015).
129. Rui, Z., Chen, L., Chen, H. & Ji, H. Strong metal-support interaction in Pt/TiO_2 induced by mild HCHO and $NaBH_4$ solution reduction and its effect on catalytic toluene combustion. *Ind. Eng. Chem. Res.* **53**, 15879–15888 (2014).
130. Gänzler, A. M. et al. Tuning the structure of platinum particles on ceria in situ for enhancing the catalytic performance of exhaust gas catalysts. *Angew. Chem. Int. Ed.* **56**, 13078–13082 (2017).
131. Gänzler, A. M. et al. Tuning the Pt/CeO_2 Interface by in situ variation of the Pt particle size. *ACS Catal.* **8**, 4800–4811 (2018).
Various reducing agents lead to different degrees of platinum nanoparticle growth and ceria reduction in Pt/CeO_2-Al_2O_3, which strongly influences the catalytic CO oxidation activity.
132. Freakley, S. J. et al. Palladium-tin catalysts for the direct synthesis of H_2O_2 with high selectivity. *Science* **351**, 965–968 (2016).
133. Hernández Mejía, C., van Deelen, T. W. & de Jong, K. P. Activity enhancement of cobalt catalysts by tuning metal-support interactions. *Nat. Commun.* **9**, 4459 (2018).
Reduction-oxidation-reduction pretreatments are applied to mitigate cobalt nanoparticle coverage by TiO_2 or Nb_2O_5 suboxides and lead to twice the exposed cobalt surface and activity in the Fischer-Tropsch synthesis.
134. Zhan, W. et al. A sacrificial coating strategy toward enhancement of metal-support interaction for ultrastable Au nanocatalysts. *J. Am. Chem. Soc.* **138**, 16130–16139 (2016).
135. Phaahlamohlaka, T. N. et al. A sinter resistant Co Fischer-Tropsch catalyst promoted with Ru and supported on titania encapsulated by mesoporous silica. *Appl. Catal. A Gen.* **552**, 129–137 (2018).
136. Li, H. et al. Evidence of the encapsulation model for strong metal–support interaction under oxidized conditions: a case study on TiO_x/Pt(111) for CO oxidation by in situ wide spectral range infrared reflection adsorption spectroscopy. *ACS Catal.* **8**, 10156–10163 (2018).
137. Weng, Z. & Zaera, F. Sub-monolayer control of mixed-oxide support composition in catalysts via atomic layer deposition: selective hydrogenation of cinnamaldehyde promoted by (SiO_2-ALD)-Pt/Al_2O_3. *ACS Catal.* **8**, 8513–8524 (2018).
138. Ro, I. et al. Role of the Cu-ZrO_2 interfacial sites for conversion of ethanol to ethyl acetate and synthesis of methanol from CO_2 and H_2. *ACS Catal.* **6**, 7040–7050 (2016).
139. Moon, S. Y., Naik, B., Jung, C.-H., Qadir, K. & Park, J. Y. Tailoring metal-oxide interfaces of oxide-encapsulated Pt/silica hybrid nanocatalysts with enhanced thermal stability. *Catal. Today* **265**, 245–253 (2016).
140. Yang, N. & Bent, S. F. Investigation of inherent differences between oxide supports in heterogeneous catalysis in the absence of structural variations. *J. Catal.* **351**, 49–58 (2017).
141. Kennedy, R. M. et al. Replication of SMSI via ALD: TiO_2 overcoats increase Pt-catalyzed acrolein hydrogenation selectivity. *Catal. Lett.* **148**, 2223–2232 (2018).
142. Zhang, J. et al. Wet-chemistry strong metal-support interactions in Titania supported Au catalysts. *J. Am. Chem. Soc.* **141**, 2975–2983 (2019).
143. Wu, L., Li, B. & Zhao, C. Direct synthesis of hydrogen and dimethoxylmethane from methanol on copper/silica catalysts with optimal Cu^+/Cu^0 sites. *ChemCatChem* **10**, 1140–1147 (2018).
144. Xu, C. et al. Interfacing with silica boosts the catalysis of copper. *Nat. Commun.* **9**, 3367 (2018).
A mesoporous SiO_2 layer over a Cu/SiO_2 catalyst increases the concentration of Cu-O-SiO_x surface sites, which doubles the intrinsic activity in ester hydrogenation and increases the selectivity towards ethylene glycol from 23 % to 96 %
145. Matsubu, J. C. et al. Adsorbate-mediated strong metal–support interactions in oxide-supported Rh catalysts. *Nat. Chem.* **9**, 120–127 (2017).
When adsorbates are present on the surface of rhodium nanoparticles prior to reduction treatment, an optimised support suboxide overlayer is generated, which steers the selectivity in CO_2 hydrogenation from predominantly CH_4 to CO.
146. Wang, X. et al. Sacrificial adsorbate strategy achieved strong metal–support interaction of stable Cu nanocatalysts. *ACS Appl. Energy Mater.* **1**, 1408–1414 (2018).
147. Kleijn, S. E. F., Lai, S. C. S., Koper, M. T. M. & Unwin, P. R. Electrochemistry of nanoparticles. *Angew. Chem. Int. Ed.* **53**, 3558–3586 (2014).
148. Vannice, M. A. The catalytic synthesis of hydrocarbons from H_2/CO mixtures over the group VIII metals: V. The catalytic behavior of silica-supported metals. *J. Catal.* **50**, 228–236 (1977).

Acknowledgements

Shell Global Solutions, the Netherlands Association for Scientific Research and Companhia Brasileira de Metalurgia e Mineração are thanked for financial support. K.P.d.J. acknowledges support from the European Research Council, EU FP7 ERC Advanced Grant no. 338846.

Author contributions

T.W.v.D. and C.H.M. contributed equally. All authors were involved in literature survey, structuring and analysis of the data and writing of the manuscript.

Competing Interests

The authors declare no competing interests.

Additional information

Supplementary information is available for this paper at https://doi.org/10.1038/s41929-019-0364-x.

Correspondence should be addressed to K.P.d.J.

Reprints and permissions information is available at www.nature.com/reprints.

Publisher's note Springer Nature remains neutral with regard to jurisdictional claims in published maps and institutional affiliations.